Cold Plasma Synthesis of High Entropy Alloys from Metal Salt Solutions

CHEE 795 Ph.D. Thesis Proposal

Isaac Triplett
ID: 261248124
Supervisors:
Prof. Pierre-Luc Girard-Lauriault
Prof. Ahmad Hamdan

Chemical Engineering
McGill University
Canada
June 2025

Contents

1 Introduction **5**

2 Background **7**
2.1 High Entropy Alloys . . . 7
2.1.1 Thermodynamic Properties . . . 7
2.1.2 Current Synthesis Methods . . . 12
2.2 Cold Plasma Synthesis . . . 13
2.2.1 Cold Plasma Synthesis with Metal Salts . . . 13
2.3 The Physics of Cold Plasma Discharges . . . 14
2.3.1 Townsend Regime . . . 14
2.3.2 Streamers . . . 15
2.3.3 Modeling Approaches . . . 15
2.4 Plasma-Liquid Interactions . . . 15
2.4.1 Direct Discharge in Liquid . . . 16
2.4.2 Chemical Interaction between Gaseous Plasma Products and Liquid-Phase Species . . . 17
2.4.3 Gas Phase Plasma with a Liquid Electrode . . . 17
2.4.4 Surface Discharge . . . 19

3 Objectives **20**

4 Implementation **21**
4.1 Using Mixing Entropy to Predict Phase Formation . . . 21
4.2 Plan A: Thin-Solution Cold Plasma Synthesis . . . 22

5 Timeline **25**

6 Anticipated Contributions to Knowledge **26**

7 Research Progress **27**
7.1 Novel Theories of Mixing Entropy . . . 27
7.1.1 Distinction Between Positional Entropy and Configurational Entropy . . . 27
7.1.2 Pressure and Volume Considerations . . . 34
7.2 An Improved Townsend Approximation . . . 34
7.2.1 The False, Unstated Assumption in the Townsend Approximation . . . 35
7.2.2 My Model . . . 37
7.2.3 Reconciling the Two Models . . . 42

7.3 Synthesis 43

List of Figures

2.1 Perfectly ordered repeating patterns of elements have the same configurational entropy as entirely separated elements. 8
2.2 A plasma discharge on the surface of a droplet at an applied voltage of -13 kV, adapted from their paper with the permission of Hamdan and Dorval.[140] 19

4.1 Thin-Solution Setup: 1) Nitrogen and Argon Gas Sources 2) High Voltage Power Source 3) G2000 High Voltage Pulse Generator 4) High Voltage Transformer 5) Gas Inlet 6) To Ground 7) Liquid Coolant Inlet 8) Liquid Coolant Outlet 9) To High Voltage 10) Gas Outlet . . 22
4.2 Reproduced with permission from Banerjee et al.[16] Schematic of the system for thin-solution cold plasma synthesis. A pin electrode sits above a circular electrode in solution with a thin layer of solution above it. In Banerjee et al.'s case, the solution was composed of alcohols; in my case, it will be an aqueous solution of metal salts. . . 23

5.1 Proposed timeline for Ph.D. project from January 2025 to April 2028. 25

7.1 Improved Townsend Model, $n_0 = 1$ 38
7.2 Improved Townsend Model, $a = 1, n_0 = 1$ 39
7.3 Improved Townsend Model, $a = 1, n_0 = 1$ 40
7.4 Improved Townsend Model, $a = 1, n_0 = 1$, exponential is $n = n_0 e^{ax}$. 41
7.5 Improved Townsend Model, $a = 1, n_0 = 1$, exponential is $n = n_0 e^{0.5ax}$ 42
7.6 10 mM $Cr(NO_3)_3$, 10 kHz, 500 ns pulse width, -20 kV 44
7.7 Negative voltage plasma synthesis methods in which the plasma acts as an electrode preferentially reduce metal ions with higher reduction potentials 45
7.8 Schematic of setup for failed HEA synthesis attempt 45
7.9 Morphology and composition of Fe nanoparticles. Carbon signal is from the carbon tape (artifact of SEM characterization). Fe nanoparticle surfaces appear to have been oxidized to hematite either during or after synthesis. This is consistent with the red color they displayed afer separation from solution via boiling. 46

List of Tables

4.1 Plasma Parameters 23

1. Introduction

As reaction rates plateau in many chemical (synthesis, energy processing) and electrochemical (water splitting, redox flow batteries, etc.) fields, finding new ways to produce model materials for catalysts cheaply and effectively becomes increasingly important.[1–4] Solid catalysts are typically designed through either surface modification or nanoparticle synthesis techniques.[5–8]

Nanoparticle catalysts are utilized for ammonia decomposition, azo-dye degradation, the catalytic conversion of carbon monoxide, direct methanol fuel cells, carbon dioxide reduction, and numerous other applications.[8] High entropy alloys are one class of nanoparticles currently being investigated for all of these applications.[8] High-entropy alloys (HEAs) are single-phase mixtures of several metals, providing a versatile platform for heterogeneous catalysis.[6,7] They are being investigated for applications in ammonia decomposition, methanol fuel cells, CO_2 reduction, and numerous other applications.[8] A particularly attractive novel use is the electrochemical conversion of captured CO_2 to formic acid (FA), a route that can simultaneously decarbonize fuels and produce a safe liquid that can be converted to electricity (direct FA fuel cells).[9] High entropy alloys are natural candidates as catalysts for a variety of applications because many stable transition states exist within the infinite combination of possible cooperating metal sites and reactants.[6,7]

High entropy alloys are also good candidates for additive manufacturing applications.[10] In his review, Tsai described high entropy alloys as possessing 'many attractive properties, such as high hardness, outstanding wear resistance, good fatigue resistance characteristics, excellent high temperature strength, good thermal stability and, in general, good oxidation and corrosion resistance.'[11] All of these properties are essential for the kind of parts made via additive manufacturing. In addition to the benefits unique to additive manufacturing, additive manufacturing allows for the production of bulk materials from nanoparticles, so that if it is possible to make nanoparticles with a given composition it is also possible to make bulk material with the same composition.

Currently, no robust, well-explored method exists that is able to create high entropy alloy nanoparticles or microparticles of any composition.

Cold plasma synthesis is a versatile electrochemical synthesis technique.[12,13] Cold plasma synthesis has been used to make metallic nanoparticles, metal oxides, alloys, hydrogen, polymers, and organic molecules.[6,14–16] Because plasma harnesses very large energies, very exotic chemistry can occur in cold plasma systems, making many nanomaterials, including high entropy alloys, natural prospects for the appli-

cation of this technology.[13]

2. Background

2.1 High Entropy Alloys

Yeh et al. first defined high entropy alloys in 2004 as equimolar alloys containing five or more elements.[17] However, since then, some have proposed expanding the definition to include alloys with three or more principal elements and to loosen the constraint of equimolar concentrations to merely significant concentrations of each principal element because compounds that fit this looser definition often display similar properties and present similar challenges for synthesis.[18]

2.1.1 Thermodynamic Properties

When chemists discuss the entropy of formation of a compound, what they are usually referring to is the entropy of the distribution of electron energies in the material. This form of entropy is important for predicting phase formation in alloys. However, in alloys, another form of entropy can exist, similar to the entropy of a mixed solution. This form of entropy has been called the 'configurational entropy' and also the 'mixing entropy' of a material.[17,19] In the context of high entropy alloys, the mixing entropy of alloys was first calculated by Yeh et al. in the first article discussing high entropy alloys as a prospective new material.[17] This calculation was carried out based on the procedure for calculating the configurational entropy of a solid described by Swalin.[20]

Here is a naive and incorrect, but elucidating derivation of the mixing entropy of a compound. The Gibbs formulation of the amount of entropy in a system per mole of single particles of a substance is:

$$S = R\Sigma w_i \log w_i \tag{2.1}$$

where R is the ideal gas constant ($8.3145 J/(molK)$) and

$$w_i = \frac{N_i}{N}. \tag{2.2}$$

Where N is the total number of particles and N_i is the number of particles in state i.

In this case, the state they are considering is merely the identity of the element, so Equation 2.1 becomes

$$S_{conf} = R\Sigma c_i \log c_i. \tag{2.3}$$

In the case of an equimolar compound, this reduces to

$$S_{conf} = R\log(n), \tag{2.4}$$

where n is the number of elements in the alloy.

The issue with this derivation is not necessarily that it is strictly incorrect but that it can be applied as easily to the system before mixing (metal powders in separate containers) as it can to the system after mixing (high entropy alloy). What follows is a correct derivation of the current theory.

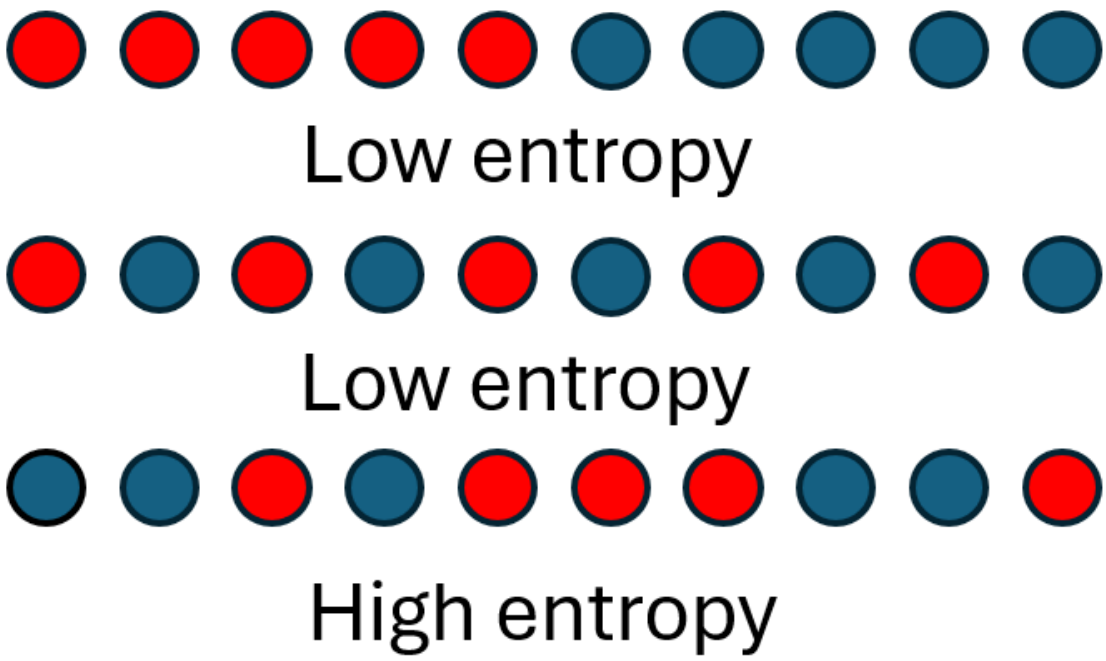

Figure 2.1: Perfectly ordered repeating patterns of elements have the same configurational entropy as entirely separated elements.

Figure 1 shows qualitatively how configurations can have different associated entropies, but to verify how configurational entropy affects phase formation, it is necessary to derive a correct method to calculate configurational entropy.

In the case of high entropy alloys with perfectly equimolar concentrations of each element, it is possible to calculate mixing entropy analytically. First, consider Boltzmann's equation:

$$S = k\log W, \tag{2.5}$$

where W is the unnormalized probability of a physical macrostate, calculated from any possible microstate resulting in the macrostate by:

$$W = N!\Pi\frac{1}{N_i!}. \tag{2.6}$$

Now, consider an equimolar alloy with n elements. Disregarding energetic constraints, what is the maximum value of W, and thus the maximum value of S, that the alloy can have? To answer this, instead of considering single atoms, it is useful to consider each state i as a cell with arbitrary but consistent orientation containing n atoms of unknown identity. Then the maximum entropy will be when the total number of states N is maximized without repetition of any state i, so that N_i is always 1. With repetition (of elements in a single state), the number of permutations possible when choosing n of n different types is simply n^n. This is the maximum value of N without any repetition of states in the microstate.

W, then, is given by:

$$W = n^n!. \tag{2.7}$$

And the entropy of a single cell is given by:

$$S = \frac{k}{n^n}\log(n^n!), \tag{2.8}$$

which, because $n^n!$ is a very large number, and because entropy only exists when a statistically significant population of microstates exists, can be simplified using Stirling's approximation[21]

$$\log(x!) = \sum_{k=1}^{x}\log k = \int_1^x \log k dk + O(\log x) = x\log x - x + 1 + O(\log x) \simeq x\log x - x \tag{2.9}$$

to

$$S = kn\log(n) - k \simeq kn\log(n). \tag{2.10}$$

This is the mixing entropy per n-sized cell, but the calculation can be verified by obtaining the same result when considering a cell containing 2n atoms. In this case

$$W = n^{2n}! \tag{2.11}$$

and

$$S = \frac{k}{n^{2n}}\log(n^{2n}!), \tag{2.12}$$

which, after applying Stirling's approximation, becomes

$$S = 2kn\log(n) - k \simeq 2kn\log(n), \tag{2.13}$$

which is the value that makes sense because the cell is twice as large.[19]

However, although a linear combination of the empirically derived mixing enthalpies of every pair of elements in the alloy and the standard deviation of elemental size have both proven to be effective characteristic values for the prediction of phase formation, mixing entropy has not.[19] Based on the current theory of mixing entropy, solid solutions with nearly equiatomic concentrations of many elements should be more thermodynamically favorable. So, the current method for calculating the mixing entropy and Gibbs free energy of mixing must be insufficient and should be modified in some way to conform to experimental evidence.

One counterargument to the claim just made about the lack of significance of mixing entropy to the thermodynamics of alloys with equimolar elemental concentrations is made by Sheng et al.[19] They showed that, while mixing entropy does not correlate with the stability of solid solution phases, it is roughly negatively proportional to the logarithm of the critical cooling rates for bulk metallic glasses.

The problem with this counterargument is that this correlation can be completely explained by kinetic arguments. Tsai et al. showed that the activation energy for self-diffusion increases with the number and uniformity of concentrations of different elements in the melt, which is all the present model of mixing entropy quantifies.[11] So, it simply requires longer for self-diffusion of atoms to crystal nucleation sites to occur in these compounds.

A more general derivation of the Bragg-Williams entropy can be achieved in the following way. Consider a set of N atoms arranged on a lattice, which can be divided into n sets of N_i *indistinguishable* atoms. The number of possible permutations of these atoms on the lattice are:

$$W = N! \prod_{i=1}^{n} \frac{1}{N_i!}. \tag{2.14}$$

So, by applying Stirling's approximation, the configurational entropy of the lattice can be found to be

$$S = k(N\log N - N) - k\sum_{i=1}^{n}[N_i \log N_i - N_i], \tag{2.15}$$

which, after expressing N_i in terms of the mole fraction x_i becomes:

$$S = -kN\sum_{i=1}^{n} x_i \log x_i, \tag{2.16}$$

which is the Bragg-Williams formulation of entropy.[22–24]

The issue with the derivation outlined just above is the reliance on the indistinguishability of atoms of a certain element. Disregarding the fact that there will be different isotopes of each element contained in the same alloy, the status of the atoms as indistinguishable is also suspicious because, unlike light, Bose-Einstein condensates, or materials that obey Fermi-Dirac statistics, they cannot be regarded as being in a regime where their de Broglie wavelengths overlap. For instance, based on the mass of nickel, the thermal de Broglie wavelength resulting from the ideal gas approximation is one order of magnitude smaller than the lattice spacing of a metal.

If one considers the atoms as distinguishable, the entropy after mixing can be derived from the absolute non-normalized probability given by:

$$W = N!, \tag{2.17}$$

which leads to

$$S_{after} = k(N \log N - N). \tag{2.18}$$

However, now, also due to the loss of indistinguishability of elements with the same atomic number, the entropy before mixing is nonzero. For it, the probability is given by:

$$W_{before} = \prod_{i=1}^{n} N_i!, \tag{2.19}$$

which leads to

$$S_{before} = k \sum_{i=1}^{n} (N_i \log N_i - N_i), \tag{2.20}$$

which, after expressing N_i in terms of the mole fraction x_i becomes:

$$S_{before} = S_{after} + kN \sum_{i=1}^{n} x_i \log x_i. \tag{2.21}$$

From this we finally obtain:

$$\Delta S = -kN \sum_{i=1}^{n} x_i \log x_i. \tag{2.22}$$

This is identical to the Bragg-Williams formulation.

2.1.2 Current Synthesis Methods

Currently, high-entropy alloys are synthesized with varying degrees of success via conventional metallurgy, hydrogen plasma synthesis with metal powders, carbonthermal shock synthesis, mechanical alloying, solvothermal synthesis, sputtering deposition, kinetically controlled laser synthesis, ultrasonication-assisted wet chemistry, dealloying, fast moving bed pyrolysis, cast cum cryo-milling, and other methods.[6–8,19,25–32]

Of these methods, the most effective are conventional metallurgy, sputtering deposition, and solvothermal synthesis.

In the case of conventional metallurgy, the synthesis of a given alloy requires that either the compound exists as a stable phase somewhere in the easily accessible temperature/pressure space, or, if trying to synthesize a glass from the melt, that the compound has a slow self-diffusion rate, a low heat capacity, a high thermal conductivity, and a high ratio of glass transition temperature to fusion temperature.[19,33] If a compound does not have these properties it will be necessary to expose them to large, conductive, and extremely cold heat sinks, which will be very expensive and may still prove insufficient in some cases.

Some of the disadvantages of conventional metallurgy have been overcome by sputtering deposition, in which the high-entropy alloy melt is sputtered directly from a high-pressure environment onto a substrate. By controlling the sputtering rate, it has been shown that sputtering deposition can create thin films with uniform metal concentrations controlled by the metal concentration in the melt.[34] However, sputtering deposition is not suitable for nanoparticle synthesis. Some researchers have attempted to synthesize nanoparticles by sputtering into an ionic liquid, but they had to tune the ionic liquid composition considerably for each different composition, were unable to synthesize nanoparticles larger than 10 nm, and the STEM-EDX images of their particles seem to show that the resulting elemental composition is not uniform.[27]

Solvothermal synthesis seems like a promising synthesis technique for some high-entropy alloy nanoparticles because the nearly instantaneous reduction of metal atoms should, in principle, allow chemists to create nanoparticles with uniform or nearly uniform elemental compositions.[26] Also, the addition of surfactants and bulky anions can be used to slow down the reaction for some elements, further tuning the composition and morphology of the final product.[35] Unfortunately, solvothermal synthesis has so far disappointed. The evidence of a uniform elemental composition (in the form of STEM-EDX scans) has remained unconvincing.[26,35] It is unclear how reducing agents are to be introduced simultaneously to metal salts without complicated convective schemes. Also, this technique cannot possibly synthesize the full spectrum of high entropy alloys because even very strong reducing agents, such as sodium borohydride, in a pH 14 solution (reduction potential of -1.24 V vs. SHE) do not have a reduction potential low enough to reduce salts like aluminum (reduction potential of -1.66 V).

2.2 Cold Plasma Synthesis

Wu et al. applied another interesting technique to try to synthesize high-entropy alloys: hydrogen plasma synthesis.[6] In this experiment, they ran a hydrogen plasma containing positive and negative ions over a hot-vacuum-dried (to solid) metal salt solution. Although the EDX analysis clearly shows that this method did not result in a uniform elemental composition, a similar method did obtain a uniform elemental composition using an ionic liquid full of metal salts a year later.[36]

Cold plasmas are defined as systems in which the temperature of the electrons differs from the temperature of the molecules in the same system. Although the electrons in the system have incredibly high energies, corresponding to thousands of Kelvin, the reaction setup for this type of plasma synthesis can be operated at low temperatures. Most often, reactions begin at room temperature, although some experiments begin at 70 or 80 ° C.[37–42]

Because cold plasma synthesis methods occur at extremely high voltages (with even DC setup voltages as high as 1 kV), very exotic chemistry can occur when the solution is exposed to the resulting charge imbalance.[13] In the case of hydrogen plasma, for instance, which is heavily studied as a reactant in other chemistries, applying very high voltages causes the creation of protons and hydride ions.[43] In the case of common alcohols exposed to AC voltages of 24 kV, methane radicals and hydrogen radicals were believed to be the main initial products, which then formed more complex hydrocarbon chains after recombination.[16]

Cold plasma synthesis setups include hollow electrode microdischarge setups, microplasma jets with external electrodes, microplasma jets with consumable electrodes, and plasma-liquid systems.[12,37,44–88] Plasma synthesis can be conducted with an alternating current (AC) or direct current (DC) setup. The benefit of alternating current plasmas are that they can be operated at much higher voltages, while direct current allows for more predictable chemistry for some setups because the direction of the charge transfer at each electrode does not rapidly alternate.

Nonthermal plasmas have applications besides synthesis. For instance, the emission of cold plasmas is currently being studied for application in jet engines.[15] However, most applications are currently chemical.

2.2.1 Cold Plasma Synthesis with Metal Salts

Plasma synthesis is also utilized to reduce metal salts. In these systems, a solution containing an anode and a metal salt is exposed to a cathodic (very high negative voltage) argon or air plasma, which propagates into the solution and reduces the metal ions while the negatively charged salts are oxidized at the anode to maintain a charge balance.[89]

2.3 The Physics of Cold Plasma Discharges

2.3.1 Townsend Regime

Circa 1897, Townsend was studying a simple system.[90] A cathode and anode were suspended in a low pressure gas, a potential was set between the two electrodes, and the cathode surface was photoionized so that electrons left the cathode and traveled through the gas to the anode, causing a measurable current to flow. After observing that the current increased exponentially with the distance between the two electrodes, Townsend proposed that the electrons must be ionizing the gas as they traveled. He also proposed that the electrons created by these collision events could themselves collide with gas molecules, causing what is now termed a Townsend avalanche.[91]

In Townsend's book *The Theory of Ionization of Gases by Collision*, he derived the framework for his quantitative model of the electron avalanches he observed in this way:

'For let n be the number of ions produced in a layer of thickness, x, measured from the negative electrode, the number n including the original n_0 ions. In passing through a path of length $\mathrm{d}x$ these ions produce $na\mathrm{d}x$ new ions by collisions, so that $\mathrm{d}n = na\mathrm{d}x$. This equation on integration gives $\log n = ax + \text{constant}$, or $n = n_0 e^{ax}$ since n_0 is the value of n corresponding to $x = 0$.'[92]

Later, he explained that the Townsend coefficient, a, must be the average number of ions produced by a traveling negative ion per unit distance.

The experiment which Townsend set up to test this was then simply to expose the cathode to a constant intensity and wavelength of light and measure the resulting current at varying distances. Since the system quickly reached steady state, the expected relation between current and distance was then simply $i = i_0 e^{ax}$, where i_0 is the elementary charge multiplied by the number of electrons generated at the cathode by the light per second. Since Townsend observed an exponential increase in current with interelectrode distance (in fact this motivated the development of his theory) he concluded that his model was correct, and so has everyone in plasma physics until now.

The Townsend approximation is a model that serves as a foundation for all of contemporary plasma physics. Giants of the field like Lozansky, Firsov, and Ebert all use Townsend scaling and Townsend ionization coefficients; methods and values derived from the Townsend approximation model; as premises and characteristic values for their models, experiments, and simulations.[93–96] However, this approximation makes an assumption that is not explicitly stated, and this assumption can be discarded for a more accurate model.

2.3.2 Streamers

A very deep, general, and modern treatment of the phenomenon of streamers can be found in the work of Ebert, as well as that of Soviet physicists Losansky and Firsov.[93–96] Simplifying the phenomenon, it can be described like this: The consequence of the electron avalanche enhances the potential at its tip and fills its interior with positive ions (at least in environments with low conductivity). When the electron avalanche is intense enough (high enough value of i_0, a, or x) the Loeb-Meek-Raether criterion is met, described by Meek in his seminal 1940 paper as *'A streamer will develop when the radial field about the positive space charge in an electron avalanche attains a value of the order of the external applied field'*.[97–102] When this criterion is reached photoelectrons are drawn into the avalanche from the surrounding medium rather than from the cathode, causing the current to be independent of the band structure of the cathode, which is the characteristic feature of streamers. Raether termed the phenomena an 'electron canal', which is a great analogy since electrons flow into the streamer from the surrounding medium the same way that water flows into a canal from city streets on a rainy day.[102]

2.3.3 Modeling Approaches

Generally, quantitative approaches to modeling plasma systems can be divided into two camps:

1. Simulations based on mass-balance equations for electrons, ions, and neutral species. These make use of empirically derived coefficients for positive (Townsend coefficients) and negative ionization by collision as well as for photoionization and recombination. Herrmann et al. has shown that this type of simulation can predict real-world behavior of plasma-liquid systems.[103,104] However, this type of simulation relies heavily on accurate values of these coefficients to make predictions. More complex and accurate models can incorporate energy balance equations and couple Maxwell's equations, although at computational cost.[105,106]

2. Boltzmann equation solvers.[107]

2.4 Plasma-Liquid Interactions

Plasma-liquid interactions are well understood for atomic liquids, like argon. In these systems, elastic interactions between electrons, ions, and neutral species are simple enough to be modeled from first principles.[108] This allows for the scattering behavior, i.e. the drift velocity as well as the energy transfer and momentum transfer mean free paths, and the effect of the scattering behavior on the thermodynamics of the system, to be completely determined as functions of the electric field and pressure. By adding a simple semi-empirical model to explain the effect of inelastic collisions on the system, like that derived for room temperature (gaseous argon) by Kruithoff and Penning, then, it should be possible to completely, quantitatively explain and predict the behavior of these systems.[109] However, for any more chemically complex systems, the elastic interactions cannot be fully modeled from first principles, forcing researchers to explain most plasma-liquid interactions qualitatively and

predict the outcomes of most plasma-liquid interactions empirically.

2.4.1 Direct Discharge in Liquid

For more than seventy years, there was great debate between those who argued that development of a gaseous phase is a prerequisite for development of an electron avalanche, like Gümtherschulze and Edler, and those who argued that it is not necessary, like Schumann and Peek.[110–114] The debate was conclusively resolved when Starikovskiy et al. developed a non-equilibrium plasma in water at low frequency and voltages as low as 27 kV, and used a fast camera to show that no bubbles were formed.[115] They also showed theoretically that ionization was favored over attachment in water for E/n ratios over 50 Td. And they showed that, for sufficiently low-density regions to form purely because of changes in fluid velocity, more orders of magnitude of energy release are required than those accessible with a benchtop plasma arc setup. Rather, the formation of bubbles can be explained by the fact that non-equilibrium plasma heats up the medium over successive discharges until the surrounding liquid boils, forming bubbles. Once bubbles are formed, breakdown preferentially occurs at the electrode-gas interface.[116] This is because electrons generally have a higher mobility in gas than in liquid, requiring less potential energy build-up to reach the kinetic energy required for ionization. This rationale could be confirmed by an experiment in which the gaseous phase in contact with the electrode had a lower electron mobility than the liquid phase in contact with the electrode, so that discharges would preferentially occur in the liquid phase.

Another mechanism for bubble formation in aqueous systems where the applied voltage is cathodic is the formation of gaseous hydrogen by hydrogen evolution. Szklarczyk showed that this decreases breakdown voltage, as the previously explained rationale would suggest.[117]

A phenomenological approach to the observation of streamers in liquid has described the phenomenon well.[114,118] Kolb et al. summarized Hebner's phenomenological description succinctly in their review: '*From the wealth of available data, Hebner identified characteristic stages or modes for the expansion of discharge precursors that are typical for the development of streamers in non-polar liquids.*[118] *For pin–plane geometries, he describes four stages for a discharge initiated from a pin cathode, starting with a micrometre long, single filament, which expands at subsonic velocities(*$\sim 10^4$ *cm* s^{-1}*) from the cathode. In a second phase, this stem branches out in a bush-like growth at about the same velocity. Eventually, a single channel reaches out towards the anode with sonic speed (phase 3), speeding up even more when approaching the anode (phase 4). For an anode pin, he describes only three modes, starting with a small structure expanding at about the same speed as its equivalent for the cathode-initiated streamer. However, this first phase changes abruptly into a more filamentary structure, propagating ten times faster (typical velocities of* 4×10^5 *cm* s^{-1}*) than that observed for the cathode case. In a third phase, the streamer propagation velocity often increases by another order of magnitude. Not all stages are always observed, and the details depend on the applied field duration and the gap distance. However, in the same electrode geometry, the progression is always significantly different for opposite polarities.*'

2.4.2 Chemical Interaction between Gaseous Plasma Products and Liquid-Phase Species

The method of plasma synthesis which has, until now, shown the most promise for generation of composition-tunable alloys with uniform elemental composition is an example of indirect exposure of liquid-phase molecules to a plasma.[36,119] In these systems, a gaseous plasma, with or without continuous gas flow, is sustained next to a liquid, and the chemical products of the gaseous plasma, like radicals and ions, as well as electrons, are allowed to diffuse or convect into the liquid phase.[120] In the case of Lee et al.'s plasma synthesis of high entropy alloys, the sustained plasma was accompanied by a continuous flow of argon and hydrogen.[36] It is unknown how this synthesis method was able to deliver strong enough reducing agents to the metal salts fast enough to form high entropy alloys with uniform composition.

2.4.3 Gas Phase Plasma with a Liquid Electrode

This is by far the most common form of plasma-liquid interaction for chemical synthesis. It is used for synthesis of metal particles, synthesis of carbon nanotubes, synthesis of fuels, and for many other purposes.[12–14,16,37–39,41,42,44–46,54,58,73–76,78,80–85,87–89,120]

Often, these processes are referred to as 'plasma electrochemistry' and the plasma is referred to as a 'plasma cathode' or 'plasma anode' because the plasma merely acts as the deliverer of a high negative or positive voltage in the form of electrons and reduced species with low reduction potentials or oxidized species with high reduction potentials that penetrate only a short distance into the liquid.[120] One advantage of these techniques is that they allow for formation of solid species in solution rather than causing nucleation at an electrode surface.

The Plasma-Liquid Interface

Unique chemical and physical phenomena can occur at the plasma-liquid interface. Interfacial phenomena include sputtering of solution-phase chemicals into the gas, penetration of plasma species into the liquid, evaporation of the solvent, excitation and ionization of liquid species by light emitted from the plasma, electron-liquid interactions, and electron solvation.[120,121] Many of these processes are not well understood, with the transport of ions across the interface known to be particularly poorly understood, especially for anions.[120,122,123] Processes which occur in gas, like secondary electron emission and excitation by electrons, also occur at the plasma-liquid interface, and are known to depend on chemical properties of the liquid like pH.[120,124] Although more research is required to understand the behavior of the electron in different solvents, the reactivity of hydrated electrons has been studied extensively.[120,125–137] The energetics and hydration shell structure of hydrated electrons is especially important for the use of plasma for chemical reduction in gas phase plasmas with liquid anodes. In systems with anodic liquid electrodes, these electrons have '*a high interfacial concentration*', and '*are both highly reactive and have an anomalously high diffusion coefficient,* $D_{298K} = 4.9 \times 10^{-5} cm^2 s^{-1}$'.[120,138]

After a discharge, the system begins to equilibrate. It is well known that in a two-phase system at equilibrium the ratio of the concentrations of a species in phase

1 to the concentration of the same species in phase 2 is given by:

$$\frac{c_1}{c_2} = \exp\left(-\frac{\Delta G_{12}}{RT}\right), \tag{2.23}$$

where c_1 and c_2 are the concentration of the species in phases 1 and 2 and

$$\Delta G_{12} = \Delta H_{12} - T\Delta S_{12}, \tag{2.24}$$

where ΔH_{12} and ΔS_{12} are the difference in enthalpy and some of the difference in entropy of the species in the different phases.[120] It is only some of the difference in entropy because it does not include the configurational entropy associated with the existence of the species in multiple phases. Equation (2.23) can be derived in the following way. Considering two possible phases, the change in Gibbs free energy between a state where all particles are in phase 1 and any state is given by the expression:

$$\Delta G = N_1(H_1 - TS_1) + N_2(H_2 - TS_2) - N(H_1 - TS_1) - T\Delta S_{conf}, \tag{2.25}$$

where N_1 is the number of particles in phase 1, N_2 is the number of particles in phase 2, H_1 is the enthalpy per particle associated with phase 1, etc., and ΔS_{conf} is the change in configurational entropy associated with the population being in multiple phases simultaneously (not to be confused with the entropy associated with the positional phase space of each phase, which can also be different for each phase). Equilibrium will be given by the minimum of this expression as a function of the relevant variable, in this case the number of particles in each phase. Rewriting the expression in terms of N_1 we get:

$$\Delta G = N_1(H_1 - TS_1) + (N - N_1)(H_2 - TS_2) - N(H_1 - TS_1) - T\Delta S_{conf}. \tag{2.26}$$

Expanding the expression for ΔS_{conf}, we consider the logarithm of the number of possible microstates in which there are N_1 particles in phase 1 and N_2 particles in phase 2:

$$\Delta S_{conf} = k_B \log\left(\frac{N!}{N_1!(N - N_1)!}\right). \tag{2.27}$$

Then,

$$\frac{\partial \Delta G}{\partial N_1} = \Delta G_{12} + k_B T \log N_1 - k_B T \log N_2. \tag{2.28}$$

And at the minimum value of the function the partial derivative is 0, so:

$$\frac{N_1}{N_2} = \exp\left(-\frac{\Delta G_{12}}{k_B T}\right). \tag{2.29}$$

2.4.4 Surface Discharge

Surface discharges are discharges in which both cathode and anode are placed at the surface of the liquid, so that the plasma travels over or through it, causing a large area of plasma liquid interface but not presenting any explicit driving force for the plasma species to travel through the liquid. However, it should not be assumed that these systems are merely gas discharges with some random diffusion of plasma species into the liquid. Some particularly interesting experiments were conducted by Lyes et al. and Hamdan and Dorval, who used discharges across a water droplet and a fast camera to show that the discharge characteristics depend on solution composition.[139,140] This is because in this type of discharge current flows between the two electrodes both via plasma processes and via migration of ions in solution, even if the electrodes are not explicitly connected to the liquid surface, as in these experiments.

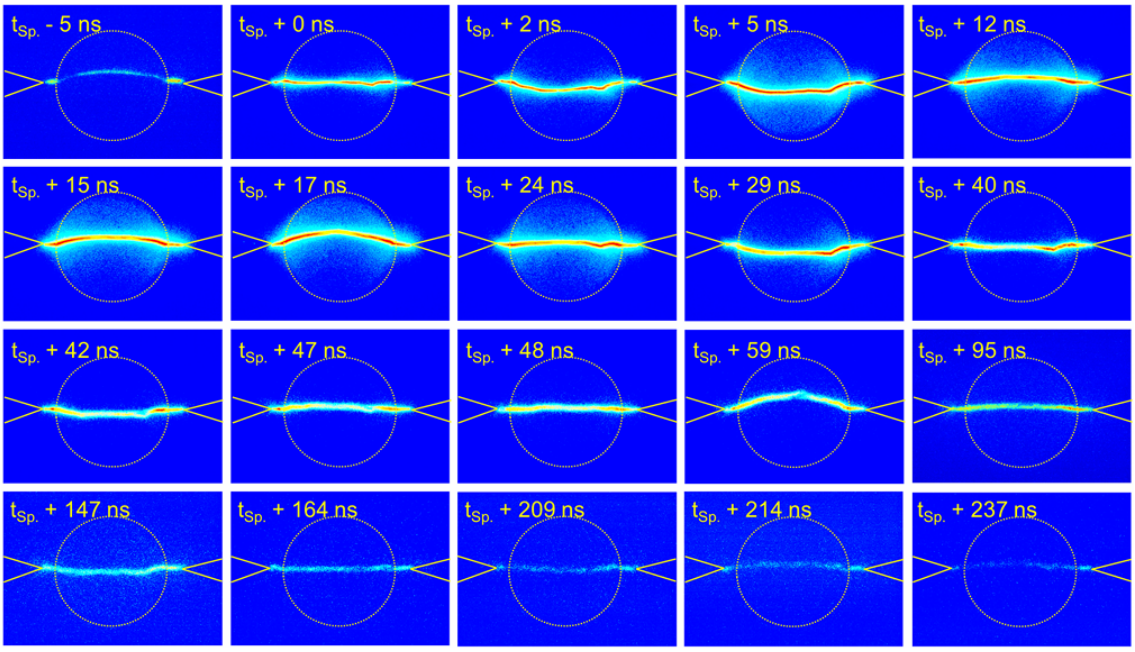

Figure 2.2: A plasma discharge on the surface of a droplet at an applied voltage of -13 kV, adapted from their paper with the permission of Hamdan and Dorval.[140]

3. Objectives

1. Use equation (4.2) to properly calculate any alloy's mixing entropy and use it to predict phase formation for Sheng et al.'s data set.[19]

2. Test a thin-solution cold plasma synthesis method (described in section 4.2) using a solution of metal salts in water to try to synthesize high entropy alloys.

3. If objective 2 is successful, expand the method to synthesize and then characterize more alloys and high entropy alloys, and optimize the synthesis method to make it as efficient as possible.

4. If objective 2 is unsuccessful, pivot to find another synthesis method for flexible alloy synthesis. Some options include:

Ambient plasma synthesis with metal salts in an ionic liquid (similar to Lee et al's method).[36]

Using a solvent with higher electron mobility and lower conductivity (water has an electron mobility of 0.002 $cm^2V^{-1}s^{-1}$ and a conductivity of $> 5.56 \times 10^{-5}$S m^{-1} at room temperature).][114,141–143]

Instead of using a plasma, avoid liquid phase ionizations by keeping the E/n ratio below 50 Td (the limit required for electrons to ionize more than they attach).[115] Instead, keep the cathode in solution and continuously shine UV rays onto the cathode surface to maximize the number of aqueous electrons.

Gaseous nanodusty synthesis.[37,47,51,52,121]

Use a high pressure environment to increase the electron density, change the breakdown voltage characteristics of the system, and decrease the mean free path (and thus the rate of ionization).[114,144–146]

5. Characterize the alloys and high entropy alloys, and optimize the synthesis method to make it as efficient as possible.

4. Implementation

4.1 Using Mixing Entropy to Predict Phase Formation

This objective will be by far the easiest and fastest to complete.

One obvious solution to determine the Gibbs free energies of various alloy phases is to start from first principles and solve the Schrodinger equation for each prospective alloy in the phase range. However, this would be extremely costly and time-consuming and may require different approximations for different alloy compositions to allow for accurate numerical solutions. As mentioned previously, a linear combination of the empirically derived mixing enthalpies of every pair of elements in the alloy and the standard deviation of elemental size have both proven to be effective characteristic values for predicting phase formation, but mixing entropy has not.[19] So, since the Gibbs free energy of the different alloys depends on the variation in size of the component elements, I could instead develop a model that incorporates the relative sizes of the different component elements.

To match empirical evidence, I can tailor the complexity of the model without making unjustified assumptions. In the simplest case, the mixing entropy of an alloy can be calculated in the same way as the mixing entropy of a gas. For a gas, the molar mixing entropy is given by

$$\Delta S_{mix} = R \sum_{i=1}^{n} x_i ln \frac{V}{V_i}, \tag{4.1}$$

where x_i is the molar fraction of gas i, V is the molar volume of the system, and V_i is the amount of molar volume inhabitable by species i. Similarly, in alloys, the issue with identifying each atom with a spot in a lattice is that different atoms have different atomic radii and thus take up different numbers of lattice spots per atom (compare Cesium with its atomic radius of 2.65 $\mathring{A}$ to Aluminum with an atomic radius of 1.432 $\mathring{A}$). So, in the case of an alloy, by substitution, the molar mixing entropy will be

$$\Delta S_{mix} = -R \sum_{i=1}^{n} x_i ln \frac{x_i v_i}{\sum_{j=1}^{n} x_j v_j}, \tag{4.2}$$

where v_i is the elemental volume of element i, as a first approximation given simply by $v_i = \frac{4}{3}\pi r_i^3$. This way, I could easily calculate the mixing entropy of all

the alloys in Sheng's study using simply the alloy formulas and the elemental sizes.[19]

This might be enough to predict phase changes effectively. If not, a more complex model could be used. Luckily, such a model already exists in a slightly different context. Flory-Huggins solution theory was developed first by Huggins and then Flory to describe the mixing Gibbs free energy, mixing enthalpy, and mixing entropy of solutions containing polymers and solvent.[147,148] The model is holistic, but puts a special statistical mechanical emphasis on the differences in size between the constituent components of the system. Flory-Huggins solution theory is generally accepted as a model capable of accurately predicting the solubility of some polymer-solution pairs.[149] It has some quirks unique to the class of systems for which it was designed, but a similar model could be developed using the same line of reasoning for other classes of systems.

The ability to quickly predict the phase formation of a wider range of alloys under different conditions will positively impact all of metallurgy.

4.2 Plan A: Thin-Solution Cold Plasma Synthesis

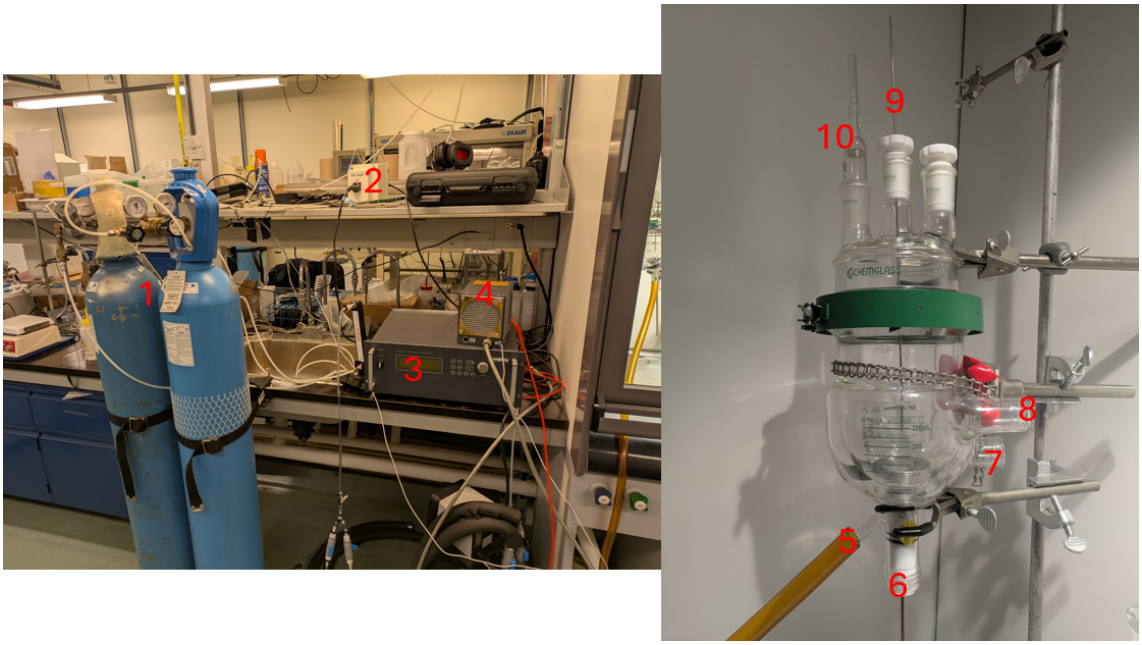

Figure 4.1: Thin-Solution Setup: 1) Nitrogen and Argon Gas Sources 2) High Voltage Power Source 3) G2000 High Voltage Pulse Generator 4) High Voltage Transformer 5) Gas Inlet 6) To Ground 7) Liquid Coolant Inlet 8) Liquid Coolant Outlet 9) To High Voltage 10) Gas Outlet

High entropy alloys will be synthesized using a setup, shown in Figure 4.1, similar to that of Banerjee et al.[16] The reaction apparatus will be continuously degassed by either argon or nitrogen (both will be tried) while being cooled to a range of different temperatures between -20 and 20 ° C. A circular plate electrode will be placed in solution and attached to ground. Above this electrode, at a height that

will vary from 2-10 mm, a pin electrode connected to high voltage will be placed, as shown in Figure 4.2. The plasma conditions to be used are given in Table 4.1.

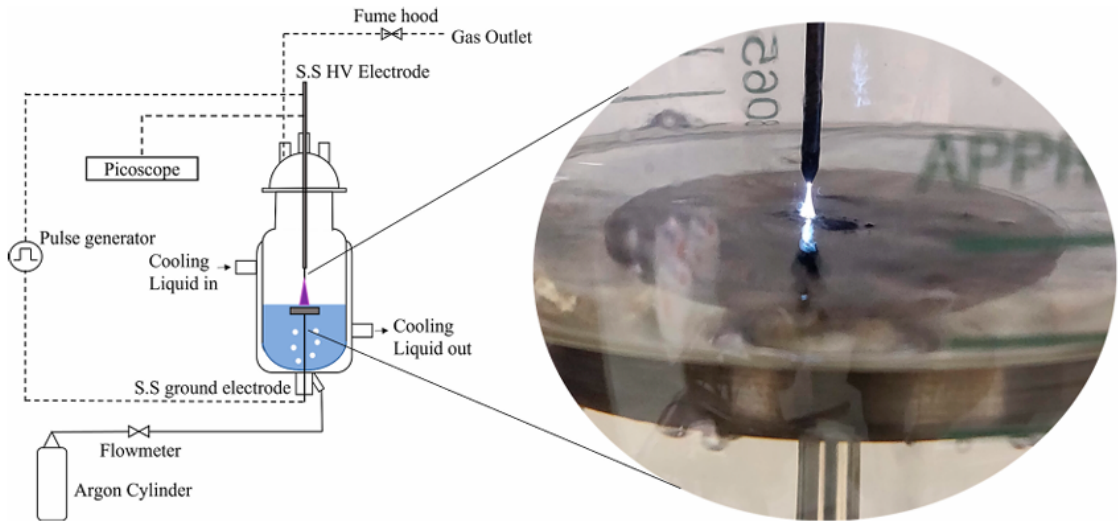

Figure 4.2: Reproduced with permission from Banerjee et al.[16] Schematic of the system for thin-solution cold plasma synthesis. A pin electrode sits above a circular electrode in solution with a thin layer of solution above it. In Banerjee et al.'s case, the solution was composed of alcohols; in my case, it will be an aqueous solution of metal salts.

Parameter	Value
Voltage (vs. gnd)	- 20 kV
frequency	10 kHz
pulse time	500 ns

Table 4.1: Plasma Parameters

Because aqueous solutions are very conductive, the high charge gradient required for maintenance of a plasma is dispersed very quickly by the solution, still causing the reduction or oxidation of some species in solution, but at a vastly lowered overpotential. In some preliminary experiments, I have not observed air plasma's penetration into pure water even at potentials as high as 20 kV. However, with a suitably high voltage and a suitably thin layer of solution between the plasma and the ground electrode, it might be possible to maintain a very high potential region of solution. Then, metal salts in that region will be reduced entirely and immediately upon exposure to plasma, and attachment with other metals will be limited by mass transport, allowing the metals to form very unstable products like high entropy alloys instead of more stable alloys with less substitution. The synthesis environment should be so extreme that the elemental composition of the product will be the same as the relative concentrations of metal salts in solution. I suspect that a similar mechanism has, in a similar method, allowed engineers to produce nanoparticles with very spherical shapes and thus very high surface areas.[150]

The particles produced by plasma synthesis are expected to be spherical, as previously reported.[89] The size of the particles is expected to decrease with increasing

electrode voltage amplitude, increase with temperature, increase with pressure, and increase with the total solution concentration of all the constituent elements of the alloy. I should be able to quickly verify these expectations during this component of the project with transmission electron microscopy.

5. Timeline

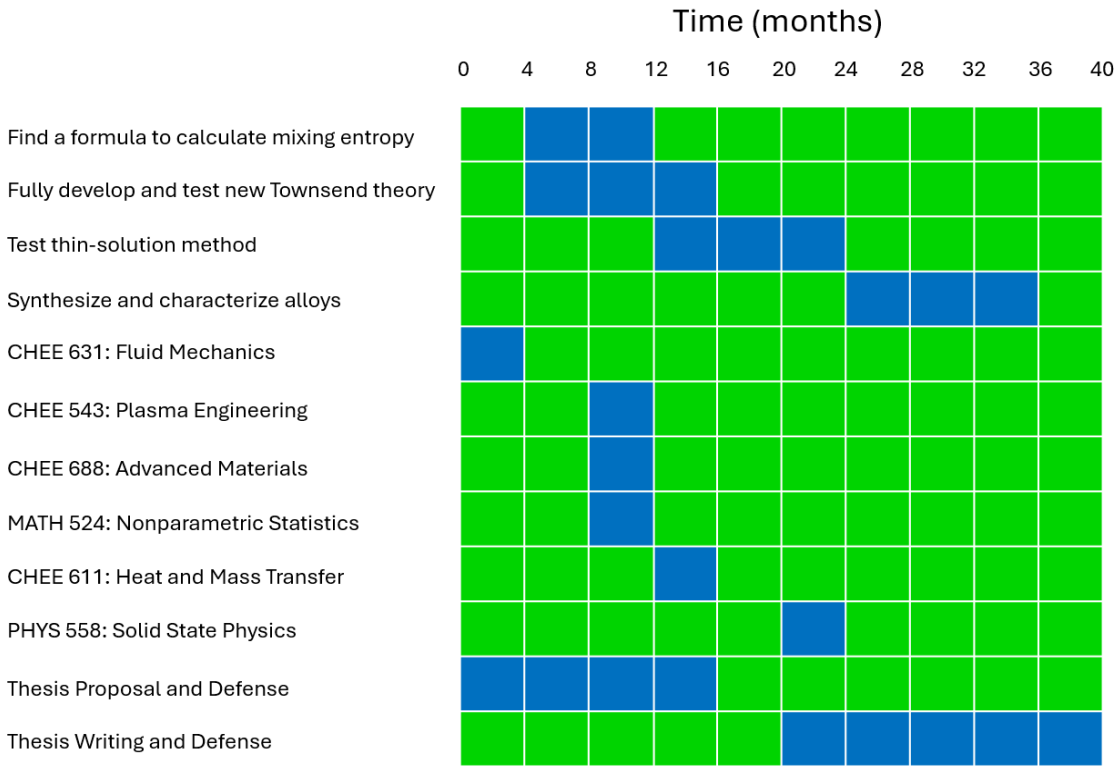

Figure 5.1: Proposed timeline for Ph.D. project from January 2025 to April 2028.

6. Anticipated Contributions to Knowledge

1. Invention of an equation or algorithm for mixing entropy and/or mixing free energy that allows for fast, approximate predictions of spontaneous alloy formation.

2. Development and implementation of a new, more accurate model of Townsend avalanches.

3. Development of a simple one-step method for the synthesis of any high entropy alloy nanoparticle.

7. Research Progress

7.1 Novel Theories of Mixing Entropy

7.1.1 Distinction Between Positional Entropy and Configurational Entropy

One can concieve of entropy in two distinct physical senses - the thermodynamic sense; which has historic priority and allows for the prediction of phase formation, free energies, and the efficiencies of processes; and the statistical mechanical sense. There is no evidence that the entropy involved in information theory, e.g. Shannon entropy, has any relation to thermodynamic entropy, besides the similarity of the mathematical formalism and the coincidental similarity to statistical mechanical entropy based on the similarity between the mathematics for probability and the mathematics for informational content.[151] Note that the connection between the thermodynamic and statistical mechanical concepts is mostly empirical. The system for which this connection has merited the most insight - that of the ideal gas - only requires that the probability of the distribution of the energies of particles be considered. Bose Einstein statistics and Fermi Dirac statistics both require that the probability of a particle having a certain energy is determined by the distribution of particles over the degenerate states associated with that energy level, but the existence of those degenerate states, in the most clear case of an ideal gas of Fermi-Dirac particles exposed to a spatially harmonic potential caused by a magnetic field, is ascribed to the energy distribution resulting from the spatial distribution rather than the spatial distribution itself.[152–156] The number of configurations of a system of atoms on a lattice may affect the possible energetic distributions of the system, but this effect will be complex, and considering the configurational possibilities without considering their energetic effects is a questionable pursuit.

Throughout Planck's magnum opus, his *Theory of Heat Radiation*, he consistently points out that his primary motivation for quantization is to be able to ascribe an absolute value to the entropy of a system.[157] The fact that the value he quantized has units implies that not all qualities of a system can have an absolute probability ascribed to them, and thus also implies that not all qualities of a system can have an absolute entropy ascribed to them.

Whether a value of the thermodynamic entropy can be derived from the positions of particles at all in all cases is not clear to me. However, instead of attempting to do away with the concept of positional entropy altogether I suggest a hypothesis which is, as I will soon show, easily falsifiable.

Hypothesis: *A thermodynamic entropy cannot be calculated from the configuration of particles, but it can be calculated from the distribution of particles in space.*

Conservation Equation for Determination of the Phase Space Size

This hypothesis is also more consistent than the current model with the most effective model for calculating the mixing entropy of ideal gases, i.e. the Sackur-Tetrode equation.[158–160] Position is defined in phase space for ideal gases, but not configuration.

However, it is more difficult to simply find the size of the phase space (in units of action) (or show that the phase space has no size) and then divide by h^{3N} in this case because the system cannot be completely defined by the positions and momenta of the atoms. However, we can make some progress:

Assuming constant temperature, we can write:

$$\sum_{j=1}^{n}\sum_{i=1}^{3N_j}\frac{\partial \dot{q}^i}{\partial t}\frac{\partial T}{\partial \dot{q}^i} = 0, \tag{7.1}$$

where T is the total kinetic energy of the system. Assuming no magnetic field, this statement is equivalent to:

$$\sum_{j=1}^{n}\sum_{i=1}^{3N_j}\dot{q}^i\frac{\partial V}{\partial q^i} = 0, \tag{7.2}$$

where V is the potential the atoms experience. If it is possible to use this and other thermodynamic constraints to define the size of the phase spece it should be possible to describe the entropy exactly.

Arbitrary Box Approach

Here is another approach. For this formulation of entropy, the equimolar case is easier to deal with and clarifying for when we later move on to the general case. Let us first calculate the entropy of the alloy after mixing. Consider N/n boxes distributed uniformly throughout the space the alloy occupies, so that each box contains n atoms. Consider each elemental identity as a distinct population. Clearly, the probability of that population's spatial distribution is maximized when each box contains one atom, and is then given by:

$$W_i = N_i! = \left(\frac{N}{n}\right)!. \tag{7.3}$$

The total probability of the system is then given by:

$$W = \prod_{i=1}^{n} N_i! = \prod_{i=1}^{n} \left(\frac{N}{n}\right)!, \tag{7.4}$$

and the entropy of the system is given by:

$$S_{after} = kN(\log N - \log n - 1). \tag{7.5}$$

Now, to calculate the entropy of the system before mixing, we confine each population to its own set of boxes, so that the number of atoms in each box is n. Then we have:

$$W_i = \frac{N_i!}{\frac{N_i}{n} n!} = \frac{N_i! n}{N_i n!}. \tag{7.6}$$

From this we can determine that:

$$S_{before} = k[N(\log N - \log n - 1) - n \log N - n^2 \log n + n^2 - \frac{1}{2} n \log(2\pi n)]. \tag{7.7}$$

Of these terms, only the first three are extensive, so it follows that:

$$\Delta S_{mix} = 0. \tag{7.8}$$

As pointed out in the background section, this is exactly what the data suggests.[19]

Now we will move on to the general case. Instead of N/n boxes, we will consider a number of boxes equal to the size of the smallest population (for an equimolar compound this is N/n). Then for W after mixing we can immediately write:

$$W = \prod_{i=1}^{n} \frac{N_i!}{N_{small} \left(\frac{N_i}{N_{small}}\right)!}, \tag{7.9}$$

from which we find that the entropy is given by:

$$S_{after} = k \sum_{i=1}^{n} \left[N_i(\log N_i - 1) - \log N_{small} - \frac{N_i}{N_{small}} \left(\log \left(\frac{N_i}{N_{small}} \right) - 1 \right) - \frac{1}{2} \log \left(2\pi \frac{N_i}{N_{small}} \right) \right] \tag{7.10}$$

Before mixing we can write:

$$W = \prod_{i=1}^{n} \frac{N_i!}{N_{small} \left(\frac{N_i}{N_{small}}\right) \left(\frac{N_{total}}{N_{small}}\right)!}, \tag{7.11}$$

from which we find that the entropy is given by:

$$S_{before} = k\sum_{i=1}^{n}[N_i(\log N_i - 1) + \log N_{total} - \log N_{small} \\ -\frac{N_{total}}{N_{small}}\left(\log\left(\frac{N_{total}}{N_{small}}\right) - 1\right) - \frac{1}{2}\log\left(2\pi\frac{N_{total}}{N_{small}}\right)] \tag{7.12}$$

After taking the difference and removing non-extensive terms we find the general formula for mixing entropy:

$$\Delta S_{mix} = k\left[n\frac{N_{total}}{N_{small}}\left(\log\left(\frac{N_{total}}{N_{small}}\right) - 1\right) - \sum_{i=1}^{n}\frac{N_i}{N_{small}}\left(\log\left(\frac{N_i}{N_{small}}\right) - 1\right)\right]. \tag{7.13}$$

This formula for the mixing entropy presents us immediately with a heuristic for falsification:

Mixing entropy is only substantial when:

$$\frac{N_{total}}{N_{small}} = O(N_{total}). \tag{7.14}$$

This is the case for some doped semiconductors, so it should be possible to test this by observing trends in phase formation when this heuristic holds.

One possible counterargument to this formulation of entropy is that Bragg-Williams entropy appears to hold for the simpler systems they consider.[22–24]

This is a good point, but one thing they specify in their paper is that any change to the order parameter (which describes the entropy) must also have a direct effect on the distribution of energies in the alloy, and on the total internal energy (and thus enthalpy) of the alloy. Thus, what appears in their case to be configurational entropy is just the entropy of the energy distribution. However, this counterargument will eventually need to be addressed in a more comprehensive analytical manner.

Another possible counterargument is that Flory-Huggins solution theory works off of similar arguments as those that describe Bragg-Williams entropy, but does not include the energy as explicitly.[22–24,147–149] This also needs a comprehensive analysis dedicated to it. Note, however, that Flory-Huggins solution theory is sometimes inconsistent at predicting solubility, especially for ternary systems, as shown by Favre et al.[149] It is interesting that this, the inclusion of more components in the system, is the same point where Bragg-Williams entropy fails.[19,161]

The main counterargument that needs to be addressed, however, is that the selection of box size changes the mixing entropy value in this model. For instance, if the number of boxes is given by the largest population of isotope, the mixing

entropy is then 0.

Or, choosing $2N_{small}$ as the number of boxes, the mixing entropy is then

$$\Delta S_{mix} = k\left[n\frac{N_{total}}{2N_{small}}\left(\log\left(\frac{N_{total}}{2N_{small}}\right)-1\right)-\sum_{i=1}^{n}\frac{N_i}{2N_{small}}\left(\log\left(\frac{N_i}{2N_{small}}\right)-1\right)\right]. \tag{7.15}$$

This arbitrariness suggests that entropy cannot be defined for position because, unlike energy or action, position cannot be quantized, as I suggested earlier. If position cannot be quantized, how can configuration?

Full Sackur-Tetrode Treatment - Extension of the Sackur-Tetrode Entropy into the Canonical Ensemble for Distributions of Particles with Different Masses and Volumes

According to Sackur-Tetrode theory, the entropy of a system can be fully determined by dividing the momentum-position phase space by h^{3N} and applying Boltzmann's formula. Starting with the energy function we have:

$$2K.E. = \sum_{i=1}^{3N}\dot{q}^i\frac{\partial\mathcal{L}}{\partial\dot{q}^i} = 3NkT \tag{7.16}$$

where T is the tempereature. Assuming that no magnetic fields are present we can then write

$$2K.E. = \sum_{j=1}^{n}\sum_{i=1}^{3N_j}\dot{q}^i m_j\dot{q}^i = 3NkT \tag{7.17}$$

or

$$2K.E. = \sum_{j=1}^{n}\frac{1}{m_j}\sum_{i=1}^{N_j}p_{ix}^2+p_{iy}^2+p_{iz}^2 = 3NkT, \tag{7.18}$$

which is the equation that describes the surface of a $3N$ dimensional hyperellipsoid:

$$\sum_{j=1}^{n}\frac{1}{3NkTm_j}\sum_{i=1}^{N_j}p_{ix}^2+p_{iy}^2+p_{iz}^2 = 1. \tag{7.19}$$

There will be other constraints on the momenta (e.g. unless you are dealing with a gas one particle cannot have all of the momentum of the system), but this gives a good upper limit to the size of the phase space as well as a good approximation for

comparison with other similar models, especially those that use the same logic. It is definitely an improvement on the current model, which does not take momentum into consideration at all.

The surface area of this hyperellipsoid is given by:

$$A = \left(\prod_{j=1}^{n} \left(\sqrt{3NkTm_j} \right)^{3N_j} \right) \frac{2\pi^{\frac{3N}{2}}}{\Gamma\left(\frac{3N}{2}\right)} \sqrt{\frac{1}{3N} \sum_{j=1}^{n} \sum_{i=1}^{3N_j} \frac{1}{\sqrt{3NkTm_j}}} \tag{7.20}$$

This is the size of the momentum phase space of the system. Now, what is the size of the position phase space of the system? For an ideal gas, this would simply be V^N. However, because metal atoms will exert a considerable potential upon each other, the volume accessible to them is much more difficult to compute. However, by staying in the canonical ensemble (the prior step did not require specification of the energy of the system) we are able to find an upper limit for the size of the phase space (and thus the value of the mixing entropy) by allowing the potential to become arbitrarily large.

Then, accounting for the indistinguishability of each element and quantizing, the total size of the phase space is:

$$\phi = \frac{\left(AV^N \prod_{i=1}^{n} \frac{1}{N_i!} \right)}{h^{3N}}, \tag{7.21}$$

and the entropy is:

$$S = k \left[N \log V + \log A - \sum_{i=1}^{n} (N_i \log N_i - N_i) - 3N \log h \right]. \tag{7.22}$$

If we consider only the positional entropy then we consider only the first term. Then the molar mixing entropy is given by equation (4.2), just as comparison of the problem to Flory-Huggins theory would suggest. This represents an upper limit, and the model could be improved by using a more sophisticated approach to calculate the size of the position phase space (perhaps making use of equation (7.2)). However, consider that this value depends only on the ratio of volume accessible to each element before and after mixing, and that this value should not change much after applying the more sophisticated model of position phase space. Also, for both position phase space and momenta phase space, consider what the limit is of the proportion of the surface area of a hypersphere at the extremes of each axis as the number of dimensions of the hypersphere increases to infinity.

One may be tempted to claim that A, the size of the momenta phase space, does not change when mixing, because in both cases a temperature can be assigned to the total system and the shape of the momenta phase space can be derived in the same way. However, this is incorrect. At thermal equilibrium (canonical ensemble), before mixing, there are n systems, each containing N_j particles, and each being

held at the temperature T, and afterwards there is one system of N particles being held at the temperature T. The ratio of the size of these two momenta phase spaces is not obvious, in the sense that it requires calculation of the entropy resulting from the size of the surface areas of the hyperellipsoid in the one case and the n hyperspheres in the other.

The entropy of each system before mixing must be evaluated independently and summed (or equivalently the phase space sizes could be multiplied). With the same logic as before, we can write:

$$\frac{1}{3N_j kTm_j}\sum_{i=1}^{N_j} p_{ix}^2 + p_{iy}^2 + p_{iz}^2 = 1. \tag{7.23}$$

This describes the surface of a hypersphere whose surface area is given by:

$$A_j = \frac{2\pi^{\frac{3N_j}{2}}(3N_j kTm_j)^{\frac{3N_j-1}{2}}}{\Gamma\left(\frac{3N_j}{2}\right)}. \tag{7.24}$$

This then gives, for the size of the phase space for each element population:

$$\phi_j(N_j, V_j, T) = \frac{V_j^{N_j}}{N_j!}A_j\frac{\delta p}{h^{3N}}, \tag{7.25}$$

where δp is the momentum uncertainty of the system, a minuscule value that vanishes upon taking the logarithm. The contribution of the momenta phase space to the mixing entropy can then by written as:

$$\begin{aligned}\log A_{total} - \sum_{j=1}^{n}\log A_j = \sum_{j=1}^{n}\frac{3N_j}{2}\log(3NkTm_j) + \frac{3N}{2}\log\pi + \log 2 \\ - \log\Gamma\left(\frac{3N}{2}\right) + \frac{1}{2}\log\left(\frac{1}{3N}\sum_{j=1}^{n}\sum_{i=1}^{N_j}\frac{1}{\sqrt{3NkTm_j}}\right) \\ -\sum_{j=1}^{n}\left[\log 2 + \frac{3N_j}{2}\log\pi + \frac{3N_j-1}{2}\log(3N_j kTm_j) + \log(\delta p_j) - \log\Gamma\left(\frac{3N_j}{2}\right)\right].\end{aligned} \tag{7.26}$$

After removing non-extensive terms and simplifying, this becomes:

$$\Delta S_{mix,momenta} = \frac{3N}{2}\log\left(\frac{3}{2}\right) \tag{7.27}$$

7.1.2 Pressure and Volume Considerations

For systems with more elements, more disorder increases the volume (and thus the enthalpy), leading to distorted phase diagrams. This could be easily tested by observing if the mixing entropy can predict phase formation in vacuum.

Bragg and Williams gave an approximation, which they claimed to be the upper limit of the effect of the pressure on the melting temperature of an alloy, as:[23]

$$\frac{\delta T}{\delta p} = \frac{T \delta v}{L}, \tag{7.28}$$

where δp and δv are the pressure and volume changes resulting from mixing and L is the latent heat of melting. So, if alloys with multiple elements change volume more when mixed (which seems reasonable), we would expect the transitions, not just to liquid but also to the solid solution from any other phases, to be displaced unfavorably for the solid solution.

This formula can easily be derived in the following way. The thermodynamic criterion for transition from one state to another can be stated like this:

$$U_1 + \delta p \delta v - T_{transition} S_1 = U_2 - T_{transition} S_2. \tag{7.29}$$

Solving for the transition temperature:

$$T_{transition} = T \left(\frac{U_2 - U_1}{L} + \frac{\delta p \delta v}{L} \right), \tag{7.30}$$

for a transition which occurs discontinuously with temperature, like a phase change. Only the second term depends on the expansion of the material, so we can write the contribution of the expansion as equation (7.28).

7.2 An Improved Townsend Approximation

It should be possible to set the minimum breakdown voltage for solutions to reasonable values (e.g. - 20 kV) simply by varying the metal salt concentrations.[36] This problem can be attacked both empirically and theoretically. Empirically, it should be sufficient to vary total metal salt concentrations, possibly vary plasma voltage, measure conductivity, and observe the resulting products. From the theoretical side, a simple model will be created to predict breakdown voltage based on solution conductivity.

The electron avalanche is conceptually tied to this breakdown voltage estimation in liquid media because it could lead to a nonlinear dependence of product composition on parameters or even the oxidation of products of the intial negative voltage and the metal salts. (This is something that I suspect could be leading to the predominance of products with high reduction potentials in the systems described in section 7.3 - oxidation of products with low reduction potentials by the positive ions following in the wake of the electron avalanche.)

7.2.1 The False, Unstated Assumption in the Townsend Approximation

The false, unstated assumption in the Townsend approximation is contained in the sentence 'in passing through a path of length dx these ions produce nadx new ions by collisions, so that d$n = na\,$dx.'[92] There are two problems with this assumption.

Inconsistency in the Definition of the Townsend Coefficient

First of all, the stated value of a, the Townsend coefficient, is the average number of ions produced by a traveling negative ion per unit distance. However, based on the simple differential formula Townsend provided, this cannot be the case. In fact, based on Townsend's model, the expected number of ionizing impact events per unit distance is $2a$. Here is why. d$n = nadx$ implies that a is the probability density function (pdf) for an ionizing impaction event to occur. A more general model, then, is $dn = nf(x)dx$, where $f(x)$ is the pdf. a is a uniform distribution, and no expected value can be derived from a uniform distribution because a uniform distribution cannot be normalized. However, we can still find the expected value. The first way to do this is to recognize that a uniform distribution is a type of symmetric distribution, and for any symmetric distribution the expected value will be the same as the median. The median of a normalized pdf is defined as the value m at which

$$\int_{-\infty}^{m} f(x)\mathrm{d}x = 0.5, \tag{7.31}$$

where $f(x)$ is the pdf. Since there is zero probability of impaction before the cathode, the lower bound becomes zero, and the expected value of the first impaction event can be found simply from

$$\int_{0}^{m} a\mathrm{d}x = 0.5 \tag{7.32}$$

to be $m = \frac{1}{2a}$. This means that each electron will be involved in $2a$ impaction events per unit distance. This can then be verified by finding the x value at which the pdf has to be artificially truncated in order to obtain an expected value of $\frac{1}{a}$. The expected value of any function $g(x)$ for a pdf $f(x)$ is given by

$$\int_{-\infty}^{\infty} g(x)f(x)\mathrm{d}x, \tag{7.33}$$

so we want to find the upper limit d such that

$$\int_{0}^{d} ax\mathrm{d}x = \frac{1}{a}. \tag{7.34}$$

Upon integration it can then be shown that this upper limit is $d = \frac{\sqrt{2}}{a}$, which is not physical. A physical bound is $\frac{2}{a}$, so the coefficient that would be required can be found by solving

$$\int_0^{\frac{2}{a}} cx\mathrm{d}x = \frac{1}{a}. \tag{7.35}$$

This gives $c = \frac{a}{2}$, as expected.

The Assumption of a Uniform Probability Density Function

As explained above, the Townsend coefficient acts in the Townsend model as a uniform probability density function across the distance from the cathode to the anode for an ionizing impaction event. If we consider why this assumption might not be sufficient, we can then make conclusions about what parameters have to be in place in order to make the assumption sufficient, and then it might be possible both to cut out any unnecessary assumptions from the model and to make physical conclusions about the systems for which the unnecessary, non-general assumption does not introduce any error.

The reason that the uniform probability density function is definitely not correct, at least not on a sufficiently small scale, is because the electron has zero chance of ionizing any gas molecules at $x = 0$, or at any point where the electron has just ionized a molecule. This is because the ionization energy comes from the kinetic energy of the electron, and the electron requires space to accelerate. Considering that the kinetic energy of the electron is what allows the electron to ionize molecules, we can make a quick and elucidating aside that, based on Marcus theory, the probability of ionization should also decrease at a sufficiently high kinetic energy (when it has had a lot of distance to accelerate).

One of the previously unelucidated inequalities which must hold for the Townsend model to hold, then, is that the length scale at which the electron accelerates to a kinetic energy at which it is able to ionize electrons from the valence orbitals of gas molecules must be much smaller than the length scale at which we expect the first ionization event to occur, or, assuming that $\frac{\mathrm{d}V}{\mathrm{d}x}$ is approximately constant (the Townsend model, and more specifically this assumption, has a lot more problems if it is not),

$$\frac{IE}{q\frac{\mathrm{d}V}{\mathrm{d}x}} << \frac{1}{2a}, \tag{7.36}$$

where IE is the ionization energy of the valence electrons in the gas, q is the elementary charge, and $\frac{IE}{q\frac{\mathrm{d}V}{\mathrm{d}x}}$ is the distance required for the electron to accelerate to the ionization energy.

I think that this inequality is probably met for the systems which Townsend studied, just based off the fact that the relation between current and the distance between the electrodes does fit an exponential well. However, there is another

reason, which I explain below, why a nearly exponential relation might hold despite the fundamental falsity of the Townsend model.

7.2.2 My Model

The correct probability density function seems difficult to find. It is a function of the kinetic energy of the electron, the level of diffusion of the electron, the temperature of the gas, the mean free path of the electrons, and also the probability of non-ionizing impaction events at different kinetic energies. What if there was a way to replace Townsend's model with a model which did not require a probability density function at all?

The unknown probability density function should still have an expected value, $\frac{1}{a}$, for the average distance between ionizing impaction events. Assuming that all electrons produce ions at an interval of $\frac{1}{a}$, we can calculate exactly how many electrons should simultaneously reach the anode due to a single electron produced by photoionization at the cathode.

First, let's consider a distance smaller than $\frac{1}{a}$. The number of electrons that reach the anode is then

$$n = 1, \tag{7.37}$$

or for n_0 simultaneous photoionization events,

$$n = n_0. \tag{7.38}$$

If we now consider a distance between $\frac{1}{a}$ and $\frac{2}{a}$, we have

$$n = n_0(1 + ax). \tag{7.39}$$

And so on with the next terms (considering the value of n at a distance between $\frac{2}{a}$ and $\frac{3}{a}$, between $\frac{3}{a}$ and $\frac{4}{a}$, etc.):

$$n = n_0 \left(1 + ax + a\left[x - \frac{1}{a}\right]\right), \tag{7.40}$$

$$n = n_0 \left(1 + ax + a\left[x - \frac{1}{a}\right] + 2a\left[x - \frac{2}{a}\right]\right), \tag{7.41}$$

$$n = n_0 \left(1 + ax + a\left[x - \frac{1}{a}\right] + 2a\left[x - \frac{2}{a}\right] + 4a\left[x - \frac{3}{a}\right]\right), \tag{7.42}$$

$$n = n_0 \left(1 + ax + a\left[x - \frac{1}{a}\right] + 2a\left[x - \frac{2}{a}\right] + 4a\left[x - \frac{3}{a}\right] + 8a\left[x - \frac{4}{a}\right]\right), \tag{7.43}$$

etc.

This series is of the form

$$n = n_0 \left(1 + ax + \sum_i 2^i a \left(x - \frac{i+1}{a}\right)\right). \tag{7.44}$$

To find the limit of the series, we can simply use the equality

$$x - \frac{i+1}{a} = 0, \tag{7.45}$$

and since we want the last ionization event to occur at an interval some multiple of $\frac{1}{a}$ from the cathode the series becomes:

$$n = n_0 \left(1 + ax + \sum_{i=0}^{i<ax-1} 2^i a \left(x - \frac{i+1}{a}\right)\right). \tag{7.46}$$

Graphing this function, we can see that it looks exponential:

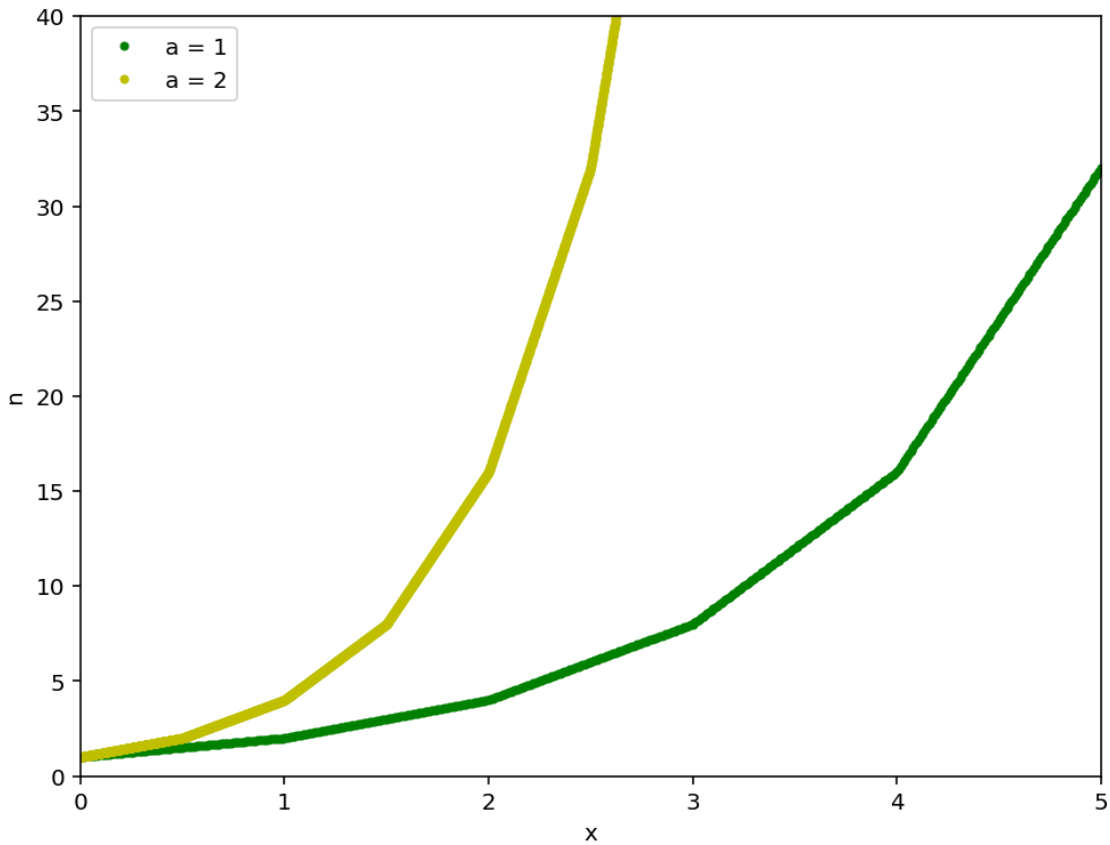

Figure 7.1: Improved Townsend Model, $n_0 = 1$

At a larger scale, it becomes indistinguishable from an exponential.

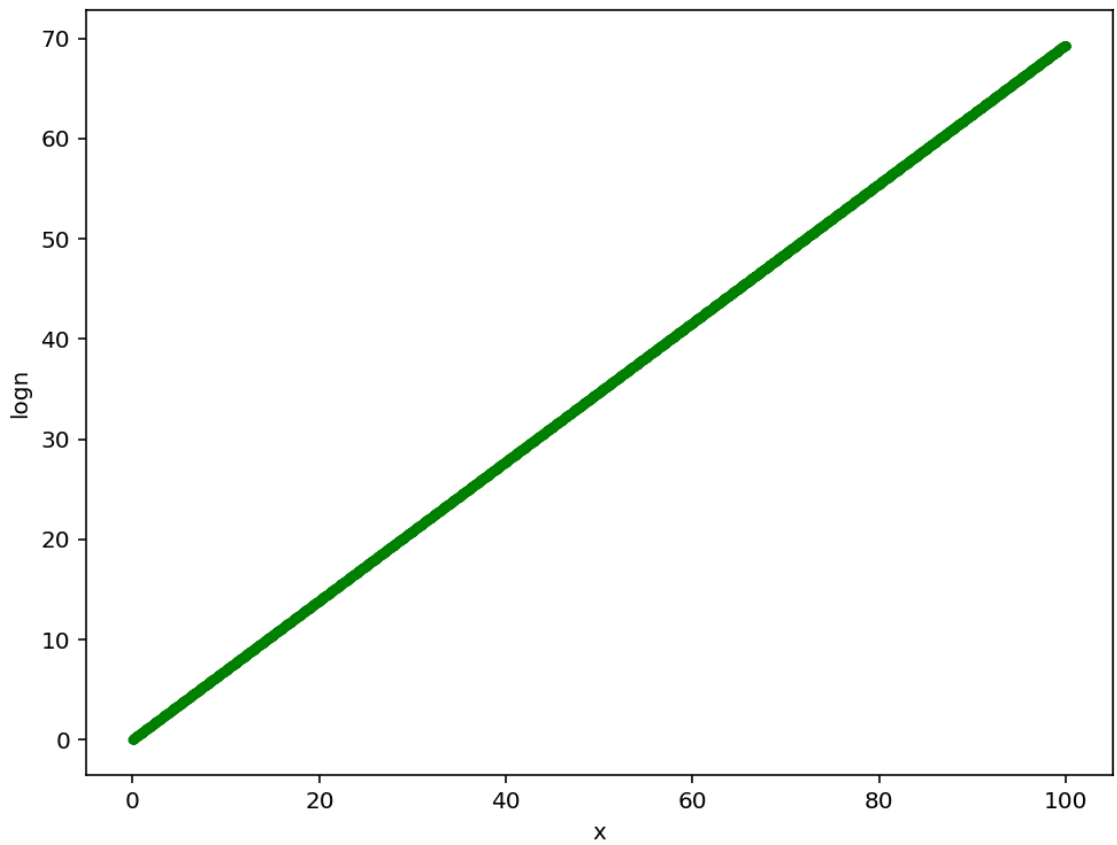

Figure 7.2: Improved Townsend Model, $a = 1, n_0 = 1$

In order to optimize numerically, and to more easily compare with the Townsend model, it is possible to make the model continuous by turning the series into an integral. That is:

$$n = n_0 \left(1 + ax + \int_0^{ax-1} 2^m a \left(x - \frac{m+1}{a} \right) \mathrm{d}m \right). \tag{7.47}$$

This can be integrated by parts to get:

$$n = n_0 \left[1 + ax - \frac{(ax-1)}{\log 2} + \frac{(2^{ax-1} - 1)}{(\log 2)^2} \right]. \tag{7.48}$$

The fact that this treatment to make the series continuous is appropriate can be verified by comparing the graphs of the discrete and continuous functions.

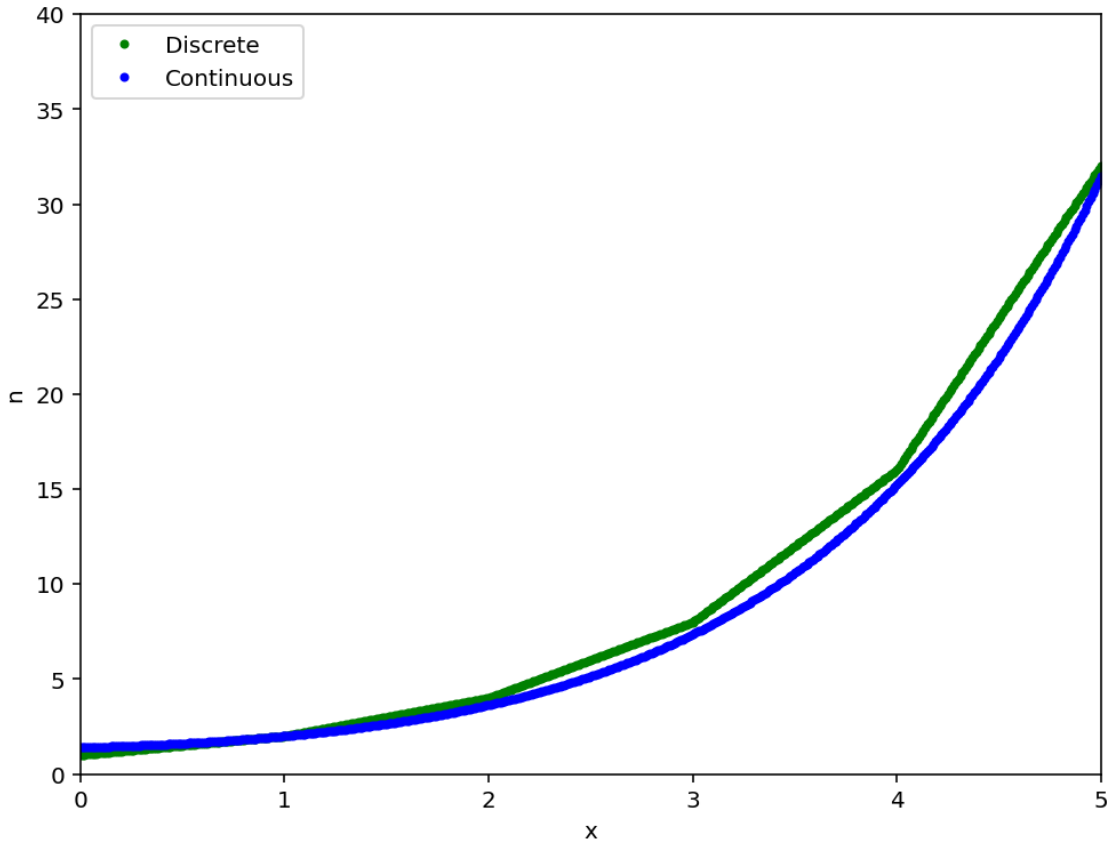

Figure 7.3: Improved Townsend Model, $a = 1, n_0 = 1$

Comparing this to the Townsend model:

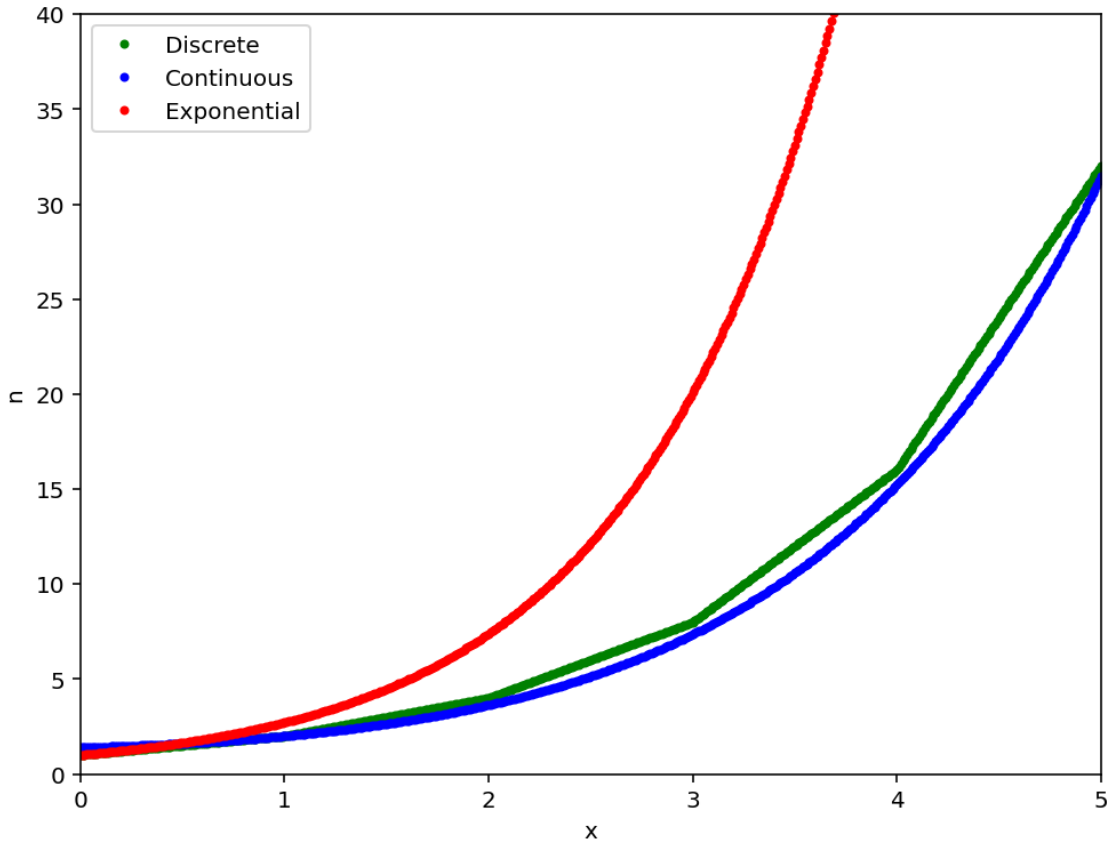

Figure 7.4: Improved Townsend Model, $a = 1, n_0 = 1$, exponential is $n = n_0 e^{ax}$

And comparing with the version of the Townsend model with an expected value for the first ionization event of $\frac{1}{a}$ (see subsection 3.1):

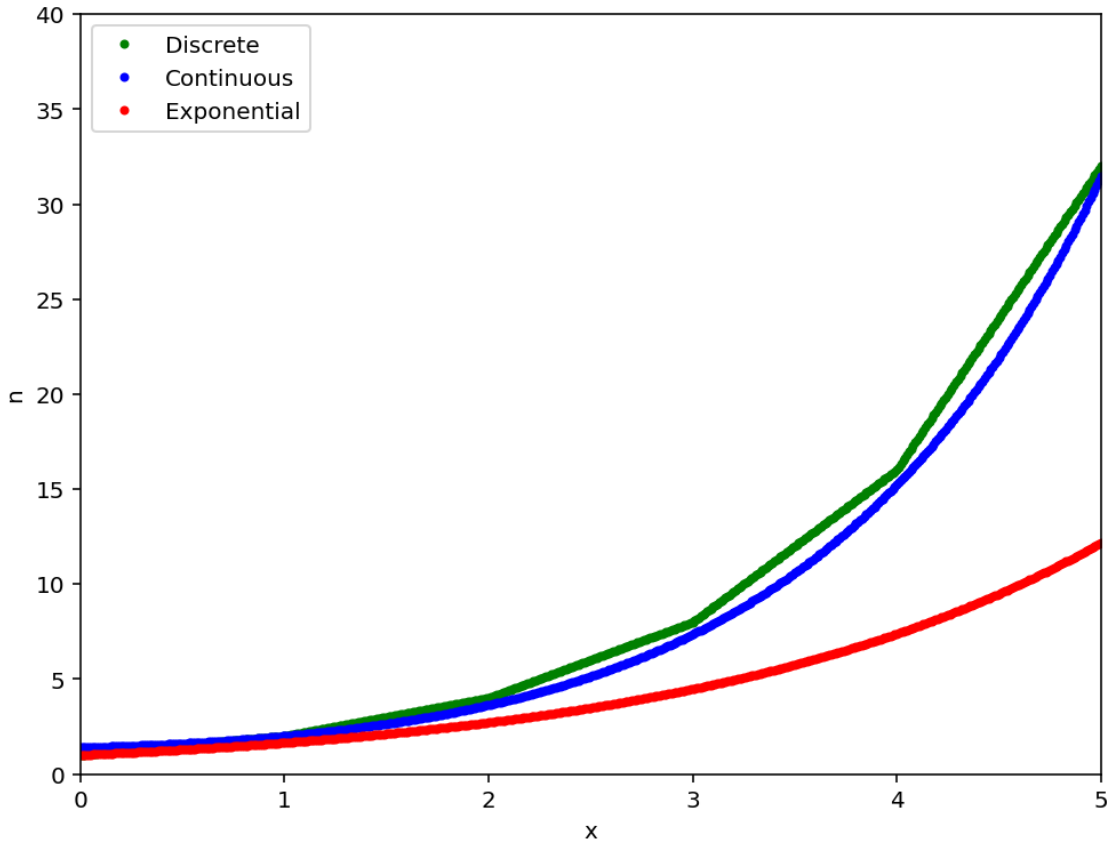

Figure 7.5: Improved Townsend Model, $a = 1, n_0 = 1$, exponential is $n = n_0 e^{0.5ax}$

7.2.3 Reconciling the Two Models

It is interesting that the same result is not obtained even when both models have the same expected value for the average interval between ionizing impaction events. It would be nice and clean to rederive Townsend's model when simplifying assumptions are made, however, the fact that both my model and Townsend's use the same number of parameters (n_0 and a) implies that neither is the simplified version of the other: rather, one is a better approximation than the other. I suspect that this inability to reconcile the two models is a unique property of the uniform pdf that Townsend used. So, I am currently working on replacing Townsend's pdf with a more physically reasonable one to see if I can rederive my result from it. The first option that sprung to mind, both for ease of integration and physical reasonableness, was an infinite series of m normal distributions with standard deviations of $\frac{1}{a}$ each centered at $\frac{m}{a}$:

$$f(x) = \sum_{m=1}^{\infty} \frac{1}{\sqrt{2\pi}} e^{-\frac{(x-\frac{m}{a})^2}{2}}. \tag{7.49}$$

This can be expanded to:

$$f(x) = \frac{a}{\sqrt{2\pi}} e^{-a^2x^2} \sum_{m=1}^{\infty} e^{amx} e^{-\frac{m^2}{2}}. \tag{7.50}$$

And, to make it easier to work with, the sum can be changed to an integral:

$$f(x) = \frac{a}{\sqrt{2\pi}} e^{-a^2x^2} \int_1^\infty e^{amx} e^{-\frac{m^2}{2}} \mathrm{d}m. \tag{7.51}$$

I integrated this with Wolfram alpha to obtain:

$$\int_1^\infty e^{amx} e^{-\frac{m^2}{2}} \mathrm{d}m = \sqrt{\frac{\pi}{2}} e^{\frac{a^2x^2}{2}} \left(\mathrm{erf}\left(\frac{ax-1}{\sqrt{2}} \right) + 1 \right). \tag{7.52}$$

This gives:

$$f(x) = \frac{a}{\sqrt{2\pi}} \sqrt{\frac{\pi}{2}} \left(\mathrm{erf}\left(\frac{ax-1}{\sqrt{2}} \right) + 1 \right). \tag{7.53}$$

I then input this pdf into Townsend's differential equation, $nf(x)\mathrm{d}x = \mathrm{d}n$ and integrated to obtain:

$$\log(n) = \frac{a}{2} \left[\int \mathrm{erf}\left(\frac{ax-1}{\sqrt{2}} \right) \mathrm{d}x + x + c \right]. \tag{7.54}$$

7.3 Synthesis

Nanoparticles have been synthesized using a variety of parameters and chemical compositions. First, Cr nanoparticles were synthesized and characterized using a high resolution scanning electron microscopy (HR-SEM) back-scattering technique. 10 mM of $Cr(NO_3)_2$ was exposed to 10 kHz 500 ns pulses of -20 kV from a Cu electrode placed 5 mm above the solution, which contained a Tungsten electrode connected to ground. The reaction at the positive electrode is most likely OER, with some possible nitrate oxidation. After 5 minutes of continuous reaction, the rate of sparks decreased drastically, and the solution's color changed from blue to green. HR-SEM images confirmed that Cr nanoparticles were produced, although they were very small and at a very low concentration.

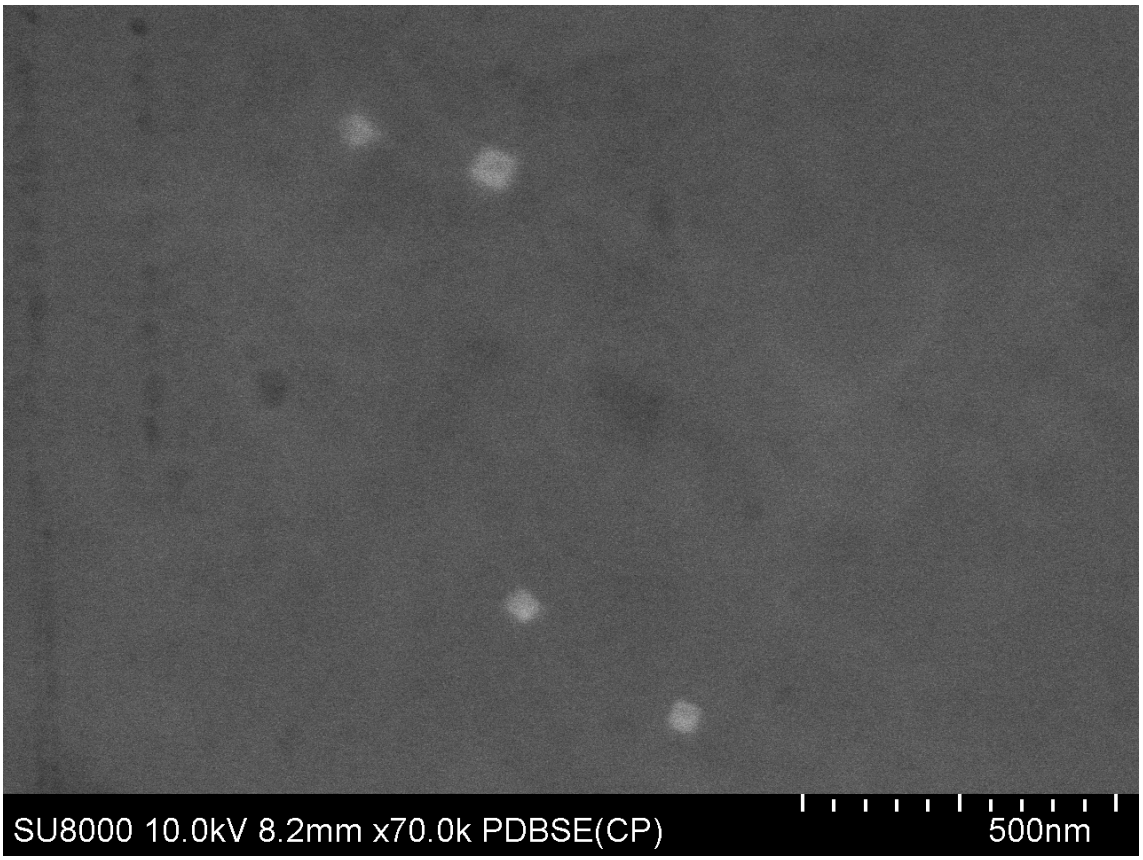

Figure 7.6: 10 mM $Cr(NO_3)_3$, 10 kHz, 500 ns pulse width, -20 kV

Another synthesis was conducted with the same parameters but with a much higher concentration of metal salts: 100 mM $AgNO_3$, 100 mM $Cr(NO_3)_2$, 100 mM $Fe(NO_3)_3$, 100 mM $Ni(NO_3)_2$, and 100 mM $Co(NO_3)_2$. At this high conductivity, the plasma acted as an electrode and only the metal salts with the most positive reduction potentials were reduced, as shown in figures 7.7 and 7.8.

Metal Reduction Potentials (vs. SHE):

Cr^{2+} + 2e -> Cr	-0.9 V
Fe^{2+} + 2e -> Fe	-0.44 V
Ni^{2+} + 2e -> Ni	-0.257 V
Ag^{+} + e -> Ag	0.7996 V
Co^{2+} + 2e -> Co	-0.28 V

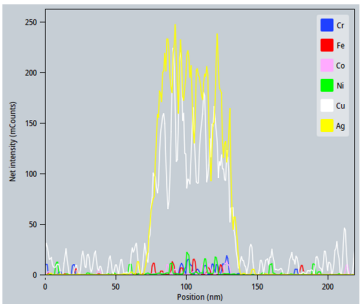

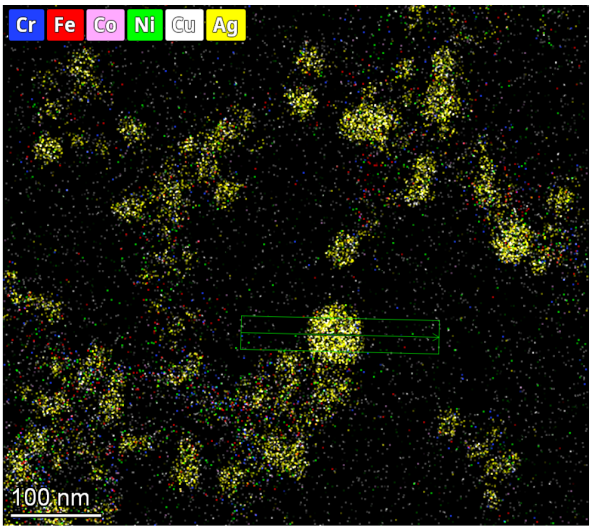

(Electrode is Cu)

Figure 7.7: Negative voltage plasma synthesis methods in which the plasma acts as an electrode preferentially reduce metal ions with higher reduction potentials

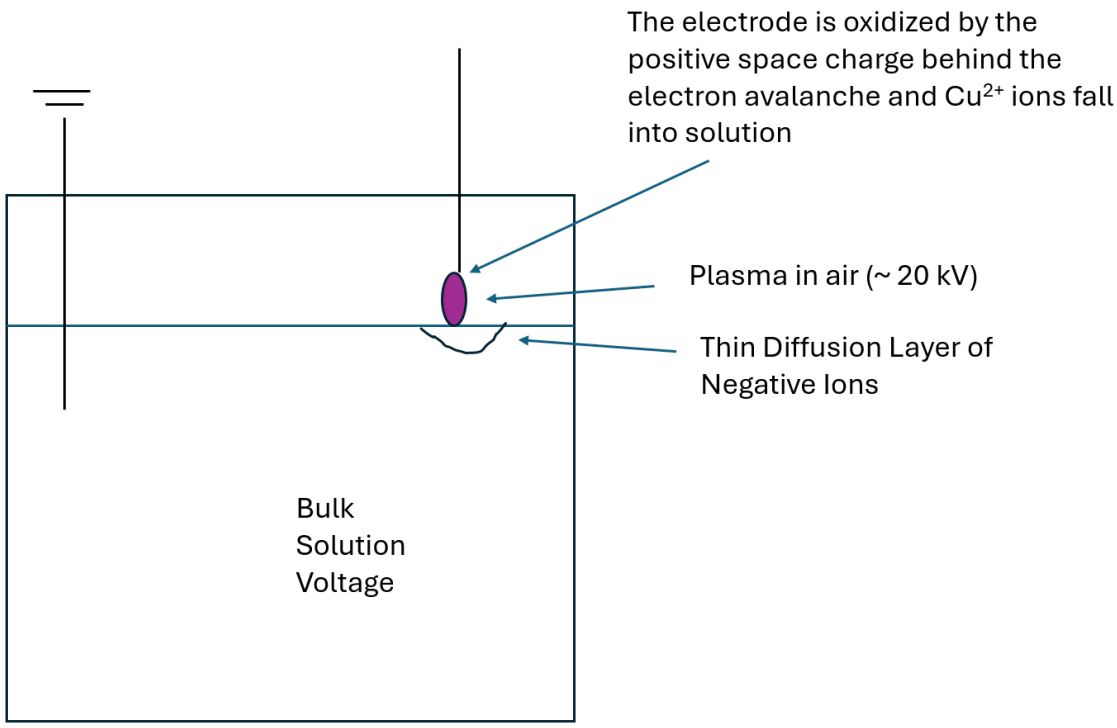

Figure 7.8: Schematic of setup for failed HEA synthesis attempt

After this failed attempt, a higher concentration of iron salt was used with the same parameters to obtain some idea of the limit of conductivity at which iron could still be reduced, and thus the limit of the size of the produced nanoparticles. 100 mM of $Fe(NO_3)_3$ was used, again in water (conductivity of metal salt solution: 25.8 mS/cm). The product morphology and composition obtained via HR-SEM and energy dispersive X-ray spectroscopy is shown in figure 7.9.

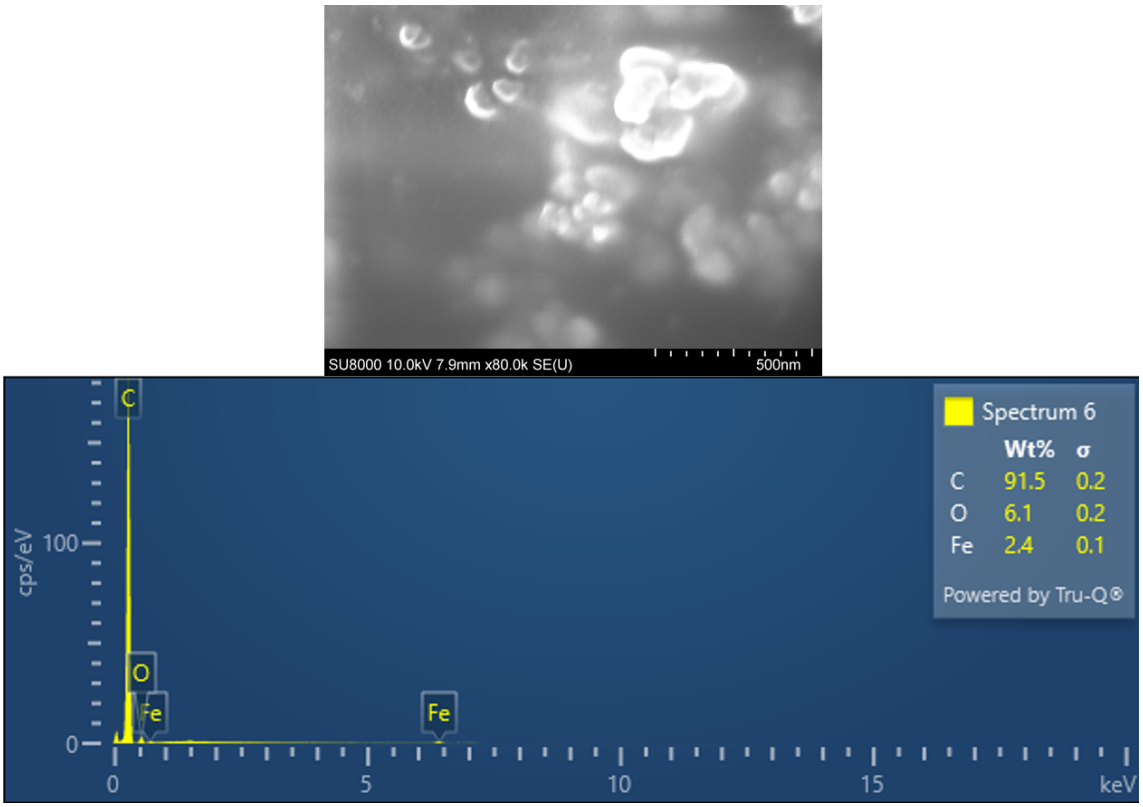

Figure 7.9: Morphology and composition of Fe nanoparticles. Carbon signal is from the carbon tape (artifact of SEM characterization). Fe nanoparticle surfaces appear to have been oxidized to hematite either during or after synthesis. This is consistent with the red color they displayed afer separation from solution via boiling.

Bibliography

(1) Mahatthananchai, J.; Dumas, A. M.; Bode, J. W. Catalytic selective synthesis. *Angewandte Chemie International Edition* **2012**, *51*, 10954–10990.

(2) Levin, O. V. Catalysts in Energy Applications, 2023.

(3) Hassan, N.; Jalil, A.; Rajendran, S.; Khusnun, N.; Bahari, M.; Johari, A.; Kamaruddin, M.; Ismail, M. Recent review and evaluation of green hydrogen production via water electrolysis for a sustainable and clean energy society. *International Journal of Hydrogen Energy* **2024**, *52*, 420–441.

(4) Gentil, S.; Reynard, D.; Girault, H. H. Aqueous organic and redox-mediated redox flow batteries: a review. *Current Opinion in Electrochemistry* **2020**, *21*, 7–13.

(5) Tharmavaram, M.; Pandey, G.; Rawtani, D. Surface modified halloysite nanotubes: A flexible interface for biological, environmental and catalytic applications. *Advances in Colloid and Interface Science* **2018**, *261*, 82–101.

(6) Wu, D.; Yao, L.; Ricci, M.; Li, J.; Xie, R.; Peng, Z. Ambient synthesis of pt-reactive metal alloy and high-entropy alloy nanocatalysts utilizing hydrogen cold plasma. *Chemistry of Materials* **2021**, *34*, 266–272.

(7) Xie, P.; Yao, Y.; Huang, Z.; Liu, Z.; Zhang, J.; Li, T.; Wang, G.; Shahbazian-Yassar, R.; Hu, L.; Wang, C. Highly efficient decomposition of ammonia using high-entropy alloy catalysts. *Nature communications* **2019**, *10*, 4011.

(8) Xin, Y.; Li, S.; Qian, Y.; Zhu, W.; Yuan, H.; Jiang, P.; Guo, R.; Wang, L. High-entropy alloys as a platform for catalysis: progress, challenges, and opportunities. *Acs Catalysis* **2020**, *10*, 11280–11306.

(9) Li, H.; Huang, H.; Chen, Y.; Lai, F.; Fu, H.; Zhang, L.; Zhang, N.; Bai, S.; Liu, T. High-entropy alloy aerogels: a new platform for carbon dioxide reduction. *Advanced Materials* **2023**, *35*, 2209242.

(10) Chen, S.; Tong, Y.; Liaw, P. K. Additive manufacturing of high-entropy alloys: a review. *Entropy* **2018**, *20*, 937.

(11) Tsai, M.-H. Physical properties of high entropy alloys. *Entropy* **2013**, *15*, 5338–5345.

(12) Lin, L.; Starostin, S. A.; Li, S.; Hessel, V. Synthesis of metallic nanoparticles by microplasma. *Physical Sciences Reviews* **2018**, *3*, 20170121.

(13) Lin, L.; Wang, Q. Microplasma: a new generation of technology for functional nanomaterial synthesis. *Plasma Chemistry and Plasma Processing* **2015**, *35*, 925–962.

(14) Zhang, J.; Wang, H.; Zhao, Q.; Di, L.; Zhang, X. Facile synthesis of PdAu/C by cold plasma for efficient dehydrogenation of formic acid. *International Journal of Hydrogen Energy* **2020**, *45*, 9624–9634.

(15) Di, L.; Zhang, J.; Zhang, X. A review on the recent progress, challenges, and perspectives of atmospheric-pressure cold plasma for preparation of supported metal catalysts. *Plasma Processes and Polymers* **2018**, *15*, 1700234.

(16) Banerjee, A.; Golsztajn, A.; Girard-Lauriault, P.-L. Plasma chemical synthesis of valuable fuels and chemicals from n-hexane and its mixture with methanol and ethanol. *ACS Sustainable Chemistry & Engineering* **2022**, *10*, 11358–11366.

(17) Yeh, J.-W.; Chen, S.-K.; Lin, S.-J.; Gan, J.-Y.; Chin, T.-S.; Shun, T.-T.; Tsau, C.-H.; Chang, S.-Y. Nanostructured high-entropy alloys with multiple principal elements: novel alloy design concepts and outcomes. *Advanced engineering materials* **2004**, *6*, 299–303.

(18) Wu, Z.; Bei, H.; Pharr, G. M.; George, E. P. Temperature dependence of the mechanical properties of equiatomic solid solution alloys with face-centered cubic crystal structures. *Acta Materialia* **2014**, *81*, 428–441.

(19) Sheng, G.; Liu, C. T. Phase stability in high entropy alloys: Formation of solid-solution phase or amorphous phase. *Progress in Natural Science: Materials International* **2011**, *21*, 433–446.

(20) Swalin, R., *Thermodynamics of Solids*; Wiley: 1991.

(21) Romik, D. Stirling's approximation for n!: The ultimate short proof? *The American Mathematical Monthly* **2000**, *107*, 556–557.

(22) Bragg, W. L.; Williams, E. J. The effect of thermal agitation on atomic arrangement in alloys. *Proceedings of the Royal Society of London. Series A, Containing Papers of a Mathematical and Physical Character* **1934**, *145*, 699–730.

(23) Bragg, W. L.; Williams, E. J. The effect of thermal agitaion on atomic arrangement in alloys—II. *Proceedings of the Royal Society of London. Series A-Mathematical and Physical Sciences* **1935**, *151*, 540–566.

(24) Williams, E. J. The effect of thermal agitation on atomic arrangement in alloys-III. *Proceedings of the Royal Society of London. Series A-Mathematical and Physical Sciences* **1935**, *152*, 231–252.

(25) Lv, Z.; Liu, X.; Jia, B.; Wang, H.; Wu, Y.; Lu, Z. Development of a novel high-entropy alloy with eminent efficiency of degrading azo dye solutions. *Scientific reports* **2016**, *6*, 34213.

(26) Bondesgaard, M.; Broge, N. L. N.; Mamakhel, A.; Bremholm, M.; Iversen, B. B. General solvothermal synthesis method for complete solubility range bimetallic and high-entropy alloy nanocatalysts. *Advanced Functional Materials* **2019**, *29*, 1905933.

(27) Löffler, T.; Meyer, H.; Savan, A.; Wilde, P.; Garzón Manjón, A.; Chen, Y.-T.; Ventosa, E.; Scheu, C.; Ludwig, A.; Schuhmann, W. Discovery of a multinary noble metal–free oxygen reduction catalyst. *Advanced Energy Materials* **2018**, *8*, 1802269.

(28) Waag, F.; Li, Y.; Ziefuß, A. R.; Bertin, E.; Kamp, M.; Duppel, V.; Marzun, G.; Kienle, L.; Barcikowski, S.; Gökce, B. Kinetically-controlled laser-synthesis of colloidal high-entropy alloy nanoparticles. *RSC advances* **2019**, *9*, 18547–18558.

(29) Liu, M.; Zhang, Z.; Okejiri, F.; Yang, S.; Zhou, S.; Dai, S. Entropy-maximized synthesis of multimetallic nanoparticle catalysts via a ultrasonication-assisted wet chemistry method under ambient conditions. *Advanced Materials Interfaces* **2019**, *6*, 1900015.

(30) Qiu, H.-J.; Fang, G.; Wen, Y.; Liu, P.; Xie, G.; Liu, X.; Sun, S. Nanoporous high-entropy alloys for highly stable and efficient catalysts. *Journal of Materials Chemistry A* **2019**, *7*, 6499–6506.

(31) Gao, S.; Hao, S.; Huang, Z.; Yuan, Y.; Han, S.; Lei, L.; Zhang, X.; Shahbazian-Yassar, R.; Lu, J. Synthesis of high-entropy alloy nanoparticles on supports by the fast moving bed pyrolysis. *Nature communications* **2020**, *11*, 2016.

(32) Kumar, N.; Tiwary, C. S.; Biswas, K. Preparation of nanocrystalline high-entropy alloys via cryomilling of cast ingots. *Journal of Materials Science* **2018**, *53*, 13411–13423.

(33) Wang, W.-H.; Dong, C.; Shek, C. Bulk metallic glasses. *Materials Science and Engineering: R: Reports* **2004**, *44*, 45–89.

(34) An, Z.; Jia, H.; Wu, Y.; Rack, P. D.; Patchen, A. D.; Liu, Y.; Ren, Y.; Li, N.; Liaw, P. K. Solid-solution CrCoCuFeNi high-entropy alloy thin films synthesized by sputter deposition. *Materials research letters* **2015**, *3*, 203–209.

(35) Lai, J.; Niu, W.; Luque, R.; Xu, G. Solvothermal synthesis of metal nanocrystals and their applications. *Nano Today* **2015**, *10*, 240–267.

(36) Lee, G.; Nguyen, N.-A.; Nguyen, V.-T.; Larina, L. L.; Chuluunbat, E.; Park, E.; Kim, J.; Choi, H.-S.; Keidar, M. High entropy alloy electrocatalyst synthesized using plasma ionic liquid reduction. *Journal of Solid State Chemistry* **2022**, *314*, 123388.

(37) Chiang, W.-H.; Richmonds, C.; Sankaran, R. M. Continuous-flow, atmospheric-pressure microplasmas: a versatile source for metal nanoparticle synthesis in the gas or liquid phase. *Plasma Sources Science and Technology* **2010**, *19*, 034011.

(38) Chang, F.-C.; Richmonds, C.; Sankaran, R. M. Microplasma-assisted growth of colloidal Ag nanoparticles for point-of-use surface-enhanced Raman scattering applications. *Journal of Vacuum Science & Technology A* **2010**, *28*, L5–L8.

(39) Du, C.; Xiao, M. Cu2O nanoparticles synthesis by microplasma. *Scientific reports* **2014**, *4*, 7339.

(40) Huang, X.; Zhong, X.; Lu, Y.; Li, Y.; Rider, A.; Furman, S.; Ostrikov, K. Plasmonic Ag nanoparticles via environment-benign atmospheric microplasma electrochemistry. *Nanotechnology* **2013**, *24*, 095604.

(41) Patel, J.; Němcová, L.; Maguire, P.; Graham, W.; Mariotti, D. Synthesis of surfactant-free electrostatically stabilized gold nanoparticles by plasma-induced liquid chemistry. *Nanotechnology* **2013**, *24*, 245604.

(42) Wang, R.; Zuo, S.; Wu, D.; Zhang, J.; Zhu, W.; Becker, K. H.; Fang, J. Microplasma-assisted synthesis of colloidal gold nanoparticles and their use in the detection of cardiac troponin I (cTn-I). *Plasma Processes and Polymers* **2015**, *12*, 380–391.

(43) Pandey, A.; Mukherjee, D.; Borah, D.; Bandyopadhyay, M.; Tyagi, H.; Yadav, R.; Chakraborty, A. Characterization of hydrogen plasma in a permanent ring magnet based helicon plasma source for negative ion source research. *Plasma Physics and Controlled Fusion* **2019**, *61*, 065003.

(44) Lin, L.; Starostin, S. A.; Li, S.; Hessel, V. Synthesis of metallic nanoparticles by microplasma. *Physical Sciences Reviews* **2018**, *3*, 20170121.

(45) Kona, S.; Kim, J.; Harnett, C.; Sunkara, M. Carbon nanotube growth studies using an atmospheric, microplasma reactor. *IEEE transactions on nanotechnology* **2008**, *8*, 286–290.

(46) Koh, T. L.; O'Hara, E. C.; Gordon, M. J. Microplasma-based synthesis of vertically aligned metal oxide nanostructures. *Nanotechnology* **2012**, *23*, 425603.

(47) Chiang, W.-H.; Sakr, M.; Gao, X. P.; Sankaran, R. M. Nanoengineering Ni x Fe1- x Catalysts for Gas-Phase, Selective Synthesis of Semiconducting Single-Walled Carbon Nanotubes. *ACS nano* **2009**, *3*, 4023–4032.

(48) Schaefer, M.; Kumar, A.; Mohan Sankaran, R.; Schlaf, R. Synthesis and in vacuo deposition of iron oxide nanoparticles by microplasma-assisted decomposition of ferrocene. *Journal of Applied Physics* **2014**, *116*.

(49) Lin, P. A.; Sankaran, R. M. Plasma-assisted dissociation of organometallic vapors for continuous, gas-phase preparation of multimetallic nanoparticles. *Angewandte Chemie-International Edition* **2011**, *50*, 10953–10956.

(50) Lin, L.; Starostin, S. A.; Hessel, V.; Wang, Q. Synthesis of iron oxide nanoparticles in microplasma under atmospheric pressure. *Chemical Engineering Science* **2017**, *168*, 360–371.

(51) Chiang, W. H.; Sankaran, R. M. Synergistic effects in bimetallic nanoparticles for low temperature carbon nanotube growth. *Advanced Materials* **2008**, *20*, 4857–4861.

(52) Chiang, W.-H.; Sankaran, R. M. In-flight dimensional tuning of metal nanoparticles by microplasma synthesis for selective production of diameter-controlled carbon nanotubes. *The Journal of Physical Chemistry C* **2008**, *112*, 17920–17925.

(53) Sankaran, R. M.; Holunga, D.; Flagan, R. C.; Giapis, K. P. Synthesis of blue luminescent Si nanoparticles using atmospheric-pressure microdischarges. *Nano letters* **2005**, *5*, 537–541.

(54) Lin, L.; Starostin, S. A.; Wang, Q.; Hessel, V. An atmospheric pressure microplasma process for continuous synthesis of titanium nitride nanoparticles. *Chemical Engineering Journal* **2017**, *321*, 447–457.

(55) Dao, V.-D.; Tran, C. Q.; Ko, S.-H.; Choi, H.-S. Dry plasma reduction to synthesize supported platinum nanoparticles for flexible dye-sensitized solar cells. *Journal of Materials Chemistry A* **2013**, *1*, 4436–4443.

(56) Li, C. J.; Sun, B. Microstructure and property of Al2O3 coating microplasma-sprayed using a novel hollow cathode torch. *Mater Lett* **2004**, *58*, 179–183.

(57) Shimizu, Y.; Sasaki, T.; Liang, C.; Bose, A. C.; Ito, T.; Terashima, K.; Koshizaki, N. Cylindrical metal wire surface coating with multiwalled carbon nanotubes by an atmospheric-pressure microplasma CVD technique. *Chem Vap Depos* **2005**, *11*, 244–249.

(58) Ghosh, S.; Liu, T.; Bilici, M.; Cole, J.; Huang, I. M.; Staack, D. Atmospheric-pressure dielectric barrier discharge with capillary injection for gas-phase nanoparticle synthesis. *J Phys D Appl Phys* **2015**, *48*, 314003.

(59) Nozaki, T.; Sasaki, K.; Ogino, T.; Asahi, D.; Okazaki, K. Microplasma synthesis of tunable photoluminescent silicon nanocrystals. *Nanotechnology* **2007**, *18*, 235603.

(60) Cao, Z.; Walsh, J. L.; Kong, M. G. Atmospheric plasma jet array in parallel electric and gas flow fields for three-dimensional surface treatment. *Appl Phys Lett* **2009**, *94*, 021501.

(61) Yang, Z.; Kikuchi, T.; Hatou, Y.; Kobayashi, T.; Shirai, H. Carbon microstructures synthesized utilizing the RF microplasma jet at atmospheric pressure. *Japanese J Appl Physics* **2005**, *44*, 4122–4127.

(62) Yoshiki, H.; Mitsui, T. TiO2 thin film coating on a capillary inner surface using atmospheric-pressure microplasma. *Surf Coatings Technol* **2008**, *202*, 5266–5270.

(63) Suzuki, T.; Kato, M.; Shimizu, Y. Fabrication of titanium-based hard coatings by atmospheric microplasma-metal organic chemical vapor deposition using titanium tetraisopropoxide. *Int J Autom Technol* **2013**, *7*, 720–725.

(64) Yoshiki, H.; Saito, T. Preparation of TiO2 thin films on the inner surface of a quartz tube using atmospheric-pressure microplasma. *J Vac Sci Technol A Vacuum, Surfaces, Film* **2008**, *26*, 338–343.

(65) Shimizu, Y.; Sasaki, T.; Ito, T.; Terashima, K.; Koshizaki, N. Fabrication of spherical carbon via UHF inductively coupled microplasma CVD. *J Phys D Appl Phys* **2003**, *36*, 2940–2944.

(66) Shimizu, Y.; Koga, K.; Sasaki, T.; Mariotti, D.; Terashima, K.; Koshizaki, N. In *Microprocess Nanotechnol 2007, 20th Int Microprocess Nanotechnol Conf MNC*, 2007, pp 174–175.

(67) Shimizu, Y.; Kawaguchi, K.; Sasaki, T.; Koshizaki, N. Generation of room-temperature atmospheric H2/Ar microplasma jet driven with pulse-modulated ultrahigh frequency and its application to gold nanoparticle preparation. *Appl Phys Lett* **2009**, *94*, 2007–2010.

(68) Shimizu, Y.; Sasaki, T.; Bose, A. C.; Terashima, K.; Koshizaki, N. Development of wire spraying for direct micro-patterning via an atmospheric-pressure UHF inductively coupled microplasma jet. *Surf Coatings Technol* **2006**, *200*, 4251–4256.

(69) Bose, A. C.; Shimizu, Y.; Mariotti, D.; Sasaki, T.; Terashima, K.; Koshizaki, N. Flow rate effect on the structure and morphology of molybdenum oxide nanoparticles deposited by atmospheric-pressure microplasma processing. *Nanotechnology* **2006**, *17*, 5976.

(70) Mariotti, D.; Lindstrom, H.; Bose, A. C.; Ostrikov, K. Monoclinic -phase nanosheets produced by atmospheric microplasma: application to lithium-ion batteries. *Nanotechnology* **2008**, *19*, 495302.

(71) Mariotti, D.; Švrček, V.; Kim, D. G. Self-organized nanostructures on atmospheric microplasma exposed surfaces. *Appl Phys Lett* **2007**, *91*, 2005–2008.

(72) Yoshiki, H.; Orada, T.; Hirai, K.; Hatakeyama, R. Growth of vertically aligned carbon nanotube bundles using atmospheric-pressure microplasma. *Japanese J Appl Physics* **2006**, *45*, 9276–9279.

(73) Shirai, N.; Uchida, S.; Tochikubo, F. Synthesis of metal nanoparticles by dual plasma electrolysis using atmospheric dc glow discharge in contact with liquid. *Jpn J Appl Phys* **2014**, *53*, 1–5.

(74) Mitra, S.; Cook, S.; Švrček, V.; Ross, A. B.; Zhou, W. Z.; Kovač, J.; Cvelbar, U.; Mariotti, D. Improved optoelectronic properties of silicon nanocrystals/polymer nanocomposites by microplasma-induced liquid chemistry. *J Phys Chem C* **2013**, *117*, 23198–23207.

(75) Huang, X.; Li, Y.; Zhong, X. Effect of experimental conditions on size control of Au nanoparticles synthesized by atmospheric microplasma electrochemistry. *Nanoscale Res Lett* **2014**, *9*, 572.

(76) Kulbe, N.; Höfft, O.; Ulbrich, A.; Abedin, S. Z. E.; Krischok, S.; Janek, J.; Polleth, M.; Endres, F. Plasma electrochemistry in 1-Butyl-3-methylimidazolium dicyanamide: Copper nanoparticles from CuCl and CuCl2. *Plasma Process Polym* **2011**, *8*, 32–37.

(77) Lee, S. W.; Zamani, H.; Feng, P. X. L.; Sankaran, R. M. Extraction of a low-current discharge from a microplasma for nanoscale patterning applications at atmospheric pressure. *J Vac Sci Technol B Microelectron Nanom Struct* **2012**, *30*, 10603.

(78) Lee, S. W.; Janyasupab, M.; Liu, C. C.; Sankaran, R. M. Fabrication of Ir nanoparticle-based biosensors by plasma electrochemical reduction for enzyme-free detection of hydrogen peroxide. *Catal Today* **2013**, *211*, 137–142.

(79) Ghosh, S.; Bishop, B.; Morrison, I.; Akolkar, R.; Scherson, D.; Sankaran, R. M. Generation of a direct-current, atmospheric-pressure microplasma at the surface of a liquid water microjet for continuous plasma-liquid processing. *J Vac Sci Technol A Vacuum, Surfaces, Film* **2015**, *33*, 21312.

(80) Huang, X. Z.; Zhong, X. X.; Lu, Y.; Li, Y. S.; Rider, A. E.; Furman, S. A.; Ostrikov, K. Plasmonic Ag nanoparticles via environment-benign atmospheric microplasma electrochemistry. *Nanotechnology* **2013**, *24*, 095604.

(81) Wang, R.; Zuo, S.; Zhu, W.; Zhang, J.; Fang, J. Rapid synthesis of aqueous-phase magnetite nanoparticles by atmospheric pressure non-thermal microplasma and their application in magnetic resonance imaging. *Plasma Process Polym* **2014**, *11*, 448–454.

(82) Imasaka, K.; Kato, Y.; Suehiro, J. Enhancement of microplasma-based water-solubilization of single-walled carbon nanotubes using gas bubbling in water. *Nanotechnology* **2007**, *18*, 335602.

(83) Saito, G.; Hosokai, S.; Tsubota, M.; Akiyama, T. Nickel nanoparticles formation from solution plasma using edge-shielded electrode. *Plasma Chem Plasma Process* **2011**, *31*, 719–728.

(84) Hattori, Y.; Mukasa, S.; Toyota, H.; Inoue, T.; Nomura, S. Synthesis of zinc and zinc oxide nanoparticles from zinc electrode using plasma in liquid. *Mater Lett* **2011**, *65*, 188–190.

(85) Lee, C. M.; Choi, S. I.; Choi, S. S.; Hong, S. H. Synthesis of boron nitride nanotubes by arc-jet plasma. *Curr Appl Phys* **2006**, *6*, 166–170.

(86) Kelgenbaeva, Z.; Omurzak, E.; Takebe, S.; Sulaimankulova, S.; Abdullaeva, Z.; Iwamoto, C.; Mashimo, T. Synthesis of pure iron nanoparticles at liquid-liquid interface using pulsed plasma. *J Nanoparticle Res* **2014**, *16*, 2603.

(87) Lee, H.; Park, S. H.; Kim, S. J.; Park, Y. K.; Kim, B. H.; Jung, S. C. Synthesis of tin and tin oxide nanoparticles using liquid phase plasma in an aqueous solution. *Microelectron Eng* **2014**, *126*, 153–157.

(88) Chen, Q.; Kitamura, T.; Saito, K.; Haruta, K.; Yamano, Y.; Ishikawa, T.; Shirai, H. Microplasma discharge in ethanol solution: Characterization and its application to the synthesis of carbon microstructures. *Thin Solid Films* **2008**, *516*, 4435–4440.

(89) Yan, T.; Zhong, X.; Rider, A. E.; Lu, Y.; Furman, S. A.; Ostrikov, K. K. Microplasma-chemical synthesis and tunable real-time plasmonic responses of alloyed Au x Ag 1- x nanoparticles. *Chemical Communications* **2014**, *50*, 3144–3147.

(90) Townsend, J. S. E. IV. The diffusion of ions into gases. *Philosophical Transactions of the Royal Society of London. Series A, Containing Papers of a Mathematical or Physical Character* **1900**, 129–158.

(91) Dion, M.; Martoff, C.; Hosack, M. On the mechanism of Townsend avalanche for negative molecular ions. *Astroparticle Physics* **2010**, *33*, 216–220.

(92) Townsend, J. S., *The Theory of Ionization of Gases by Collision*; London, Constable and Company, ltd.: 1910.

(93) Lozanski Development of electron avalances and streamers. *Soviet Physics Uspekhi* **1975**, *18*, 893.

(94) Lozansky, E.; Firsov, O. Theory of the initial stage of streamer propagation. *Journal of Physics D: Applied Physics* **1973**, *6*, 976.

(95) Ebert, U.; Nijdam, S.; Li, C.; Luque, A.; Briels, T.; van Veldhuizen, E. Review of recent results on streamer discharges and discussion of their relevance for sprites and lightning. *Journal of Geophysical Research: Space Physics* **2010**, *115*.

(96) Meulenbroek, B.; Rocco, A.; Ebert, U. Streamer branching rationalized by conformal mapping techniques. *Physical Review E—Statistical, Nonlinear, and Soft Matter Physics* **2004**, *69*, 067402.

(97) Meek, J. A theory of spark discharge. *Physical review* **1940**, *57*, 722.

(98) Loeb, L. B. Fundamental processes of electrical discharge in gases. *(No Title)* **1939**.

(99) Loeb, L. B.; Meek, J. M. The mechanism of spark discharge in air at atmospheric pressure. I. *Journal of applied physics* **1940**, *11*, 438–447.

(100) Loeb, L. B.; Meek, J. M., *The mechanism of the electric spark*; Stanford University Press: 1941.

(101) Raether, H. Über eine gasionisierende Strahlung einer Funkenentladung. *Zeitschrift für Physik* **1938**, *110*, 611–624.

(102) Raether, H. Zur entwicklung von kanalentladungen. *Archiv für Elektrotechnik* **1940**, *34*, 49–56.

(103) Herrmann, A.; Margot, J.; Hamdan, A. Experimental and 2D fluid simulation of a streamer discharge in air over a water surface. *Plasma Sources Science and Technology* **2024**, *33*, 025022.

(104) Herrmann, A.; Margot, J.; Hamdan, A. Experimental investigation and 2D fluid simulation of a positive nanosecond discharge in air in contact with liquid at various dielectric permittivity and electrical conductivity values. *Plasma Sources Science and Technology* **2024**, *33*, 125009.

(105) Nam, J. H.; Timilsina, A.; Bruggeman, P. J. Plasma Electrochemical Synthesis of Composition Tunable Au–Ag Bimetallic Nanoparticles. *The Journal of Physical Chemistry C* **2025**.

(106) Simeni, M. S.; Zheng, Y.; Barnat, E. V.; Bruggeman, P. J. Townsend to glow discharge transition for a nanosecond pulse plasma in helium: space charge formation and resulting electric field dynamics. *Plasma Sources Science and Technology* **2021**, *30*, 055004.

(107) Hagelaar, G.; Pitchford, L. C. Solving the Boltzmann equation to obtain electron transport coefficients and rate coefficients for fluid models. *Plasma sources science and technology* **2005**, *14*, 722.

(108) Lekner, J. Motion of electrons in liquid argon. *Physical Review* **1967**, *158*, 130.

(109) Kruithof, A.; Penning, F. Determination of the Townsend ionization coefficient α for pure argon. *Physica* **1936**, *3*, 515–533.

(110) Güntherschulze, A. Theory of non-ionizing breakdown in insulating liquids. *Jahrbuch der Radioaktivität und Elektronik* **1922**, 92.

(111) Edler, H. Über den Einfluß von gelöster Luft auf die Leitfähigkeit und die Durchschlagsfestigkeit vom Öl bei unsymmetrischen Elektroden und verschiedenen Drucken. *Archiv für Elektrotechnik* **1931**, *25*, 447–452.

(112) Nikuradse, A. In *Das flüssige Dielektrikum (Isolierende Flüssigkeiten)*; Springer: 1934, pp 59–157.

(113) Peek, F. W., *Dielectric phenomena in high-voltage engineering*; McGraw-Hill Book Company, Incorporated: 1929.

(114) Kolb, J.; Joshi, R.; Xiao, S.; Schoenbach, K. Streamers in water and other dielectric liquids. *Journal of Physics D: Applied Physics* **2008**, *41*, 234007.

(115) Starikovskiy, A.; Yang, Y.; Cho, Y. I.; Fridman, A. Non-equilibrium plasma in liquid water: dynamics of generation and quenching. *Plasma Sources Science and Technology* **2011**, *20*, 024003.

(116) Korobeynikov, S.; Melekhov, A. In *Proceedings of 2002 IEEE 14th International Conference on Dielectric Liquids. ICDL 2002 (Cat. No. 02CH37319)*, 2002, pp 127–130.

(117) Szklarczyk, M.; Kainthla, R. C.; Bockris, J. O. On the dielectric breakdown of water: an electrochemical approach. *Journal of The Electrochemical Society* **1989**, *136*, 2512.

(118) Hebner, R. E. In *The liquid state and its electrical properties*; Springer: 1988, pp 519–537.

(119) Tran, Q. C.; Dao, V.-D.; Kim, H. Y.; Jung, K.-D.; Choi, H.-S. Pt-based alloy/carbon black nanohybrid covered with ionic liquid supramolecules as an efficient catalyst for oxygen reduction reactions. *Applied Catalysis B: Environmental* **2017**, *204*, 365–373.

(120) Bruggeman, P. J.; Kushner, M. J.; Locke, B. R.; Gardeniers, J. G.; Graham, W.; Graves, D. B.; Hofman-Caris, R.; Maric, D.; Reid, J. P.; Ceriani, E., et al. Plasma–liquid interactions: a review and roadmap. *Plasma sources science and technology* **2016**, *25*, 053002.

(121) Samukawa, S.; Hori, M.; Rauf, S.; Tachibana, K.; Bruggeman, P.; Kroesen, G.; Whitehead, J. C.; Murphy, A. B.; Gutsol, A. F.; Starikovskaia, S., et al. The 2012 plasma roadmap. *Journal of Physics D: Applied Physics* **2012**, *45*, 253001.

(122) Jungwirth, P.; Tobias, D. J. Ions at the air/water interface, 2002.

(123) Mussard, M. D. V. S.; Foucher, E.; Rousseau, A. Charge and energy transferred from a plasma jet to liquid and dielectric surfaces. *Journal of Physics D: Applied Physics* **2015**, *48*, 424003.

(124) Cserfalvi, T.; Mezei, P. Operating mechanism of the electrolyte cathode atmospheric glow discharge. *Fresenius' journal of analytical chemistry* **1996**, *355*, 813–819.

(125) Buxton, G. V.; Greenstock, C. L.; Phillips Helman, W.; Ross, A. B. Critical review of rate constants for reacitons of hydrated electrons. *J. Phys. Chem. Ref. Data;(United States)* **1988**, *17*.

(126) Garrett, B. C.; Dixon, D. A.; Camaioni, D. M.; Chipman, D. M.; Johnson, M. A.; Jonah, C. D.; Kimmel, G. A.; Miller, J. H.; Rescigno, T. N.; Rossky, P. J., et al. Role of water in electron-initiated processes and radical chemistry: Issues and scientific advances. *Chemical reviews* **2004**, *105*, 355–390.

(127) Siefermann, K. R.; Liu, Y.; Lugovoy, E.; Link, O.; Faubel, M.; Buck, U.; Winter, B.; Abel, B. Binding energies, lifetimes and implications of bulk and interface solvated electrons in water. *Nature chemistry* **2010**, *2*, 274–279.

(128) Lübcke, A.; Buchner, F.; Heine, N.; Hertel, I. V.; Schultz, T. Time-resolved photoelectron spectroscopy of solvated electrons in aqueous NaI solution. *Physical Chemistry Chemical Physics* **2010**, *12*, 14629–14634.

(129) Shreve, A. T.; Yen, T. A.; Neumark, D. M. Photoelectron spectroscopy of hydrated electrons. *Chemical Physics Letters* **2010**, *493*, 216–219.

(130) Tang, Y.; Shen, H.; Sekiguchi, K.; Kurahashi, N.; Mizuno, T.; Suzuki, Y.-I.; Suzuki, T. Direct measurement of vertical binding energy of a hydrated electron. *Physical Chemistry Chemical Physics* **2010**, *12*, 3653–3655.

(131) Uhlig, F.; Marsalek, O.; Jungwirth, P. Unraveling the complex nature of the hydrated electron. *The Journal of Physical Chemistry Letters* **2012**, *3*, 3071–3075.

(132) Uhlig, F.; Marsalek, O.; Jungwirth, P. Electron at the surface of water: Dehydrated or not? *The journal of physical chemistry letters* **2013**, *4*, 338–343.

(133) Jacobson, L. D.; Herbert, J. M. Theoretical characterization of four distinct isomer types in hydrated-electron clusters, and proposed assignments for photoelectron spectra of water cluster anions. *Journal of the American Chemical Society* **2011**, *133*, 19889–19899.

(134) Marsalek, O.; Uhlig, F.; Vandevondele, J.; Jungwirth, P. Structure, dynamics, and reactivity of hydrated electrons by ab initio molecular dynamics. *Accounts of chemical research* **2012**, *45*, 23–32.

(135) Sagar, D.; Bain, C. D.; Verlet, J. R. Hydrated electrons at the water/air interface. *Journal of the American Chemical Society* **2010**, *132*, 6917–6919.

(136) Faubel, M.; Steiner, B.; Toennies, J. P. Photoelectron spectroscopy of liquid water, some alcohols, and pure nonane in free micro jets. *The Journal of chemical physics* **1997**, *106*, 9013–9031.

(137) Marsalek, O.; Uhlig, F.; Frigato, T.; Schmidt, B.; Jungwirth, P. Dynamics of electron localization in warm versus cold water clusters. *Physical review letters* **2010**, *105*, 043002.

(138) Rumbach, P.; Bartels, D. M.; Sankaran, R. M.; Go, D. B. The solvation of electrons by an atmospheric-pressure plasma. *Nature communications* **2015**, *6*, 7248.

(139) Sebih, L.; Carbone, E.; Hamdan, A. Electrical and optical characteristics of a nanosecond pulsed electrical discharge in air in contact with a water droplet for various electrical conductivities. *Journal of Physics D: Applied Physics* **2024**, *58*, 045206.

(140) Hamdan, A.; Dorval, A. Spatial and temporal dynamics of single nanosecond discharges in air with water droplets. *Journal of Physics D: Applied Physics* **2023**, *56*, 215202.

(141) Zahn, M.; Takada, T.; Voldman, S. Kerr electro-optic field mapping measurements in water using parallel cylindrical electrodes. *Journal of applied physics* **1983**, *54*, 4749–4761.

(142) Lide, D. R. Handbook of chemistry and physics, 2006.

(143) Wetz, D. A.; Mankowski, J. J.; Dickens, J. C.; Kristiansen, M. The impact of field enhancements and charge injection on the pulsed breakdown strength of water. *IEEE transactions on plasma science* **2006**, *34*, 1670–1679.

(144) Messerschmitt, J.; Kunhardt, E. In *Ninth IEEE International Pulsed Power Conference*, 1993; Vol. 1, p 56.

(145) Loeb, L. B. The threshold for spark development by streamer mechanism in uniform fields. *Physical Review* **1948**, *74*, 210.

(146) Miller, C. G.; Loeb, L. B. Spark breakdown at atmospheric pressure and above in relation to paschen's law. *Physical Review* **1948**, *73*, 84.

(147) Huggins, M. L. Theory of solutions of high polymers1. *Journal of the American Chemical Society* **1942**, *64*, 1712–1719.

(148) Flory, P. J. Thermodynamics of high polymer solutions. *The Journal of chemical physics* **1942**, *10*, 51–61.

(149) Favre, E.; Nguyen, Q.; Clement, R.; Neel, J. Application of Flory-Huggins theory to ternary polymer-solvents equilibria: A case study. *European polymer journal* **1996**, *32*, 303–309.

(150) Panomsuwan, G.; Watthanaphanit, A.; Ishizaki, T.; Saito, N. Water-plasma-assisted synthesis of black titania spheres with efficient visible-light photocatalytic activity. *Physical Chemistry Chemical Physics* **2015**, *17*, 13794–13799.

(151) Shannon, C. E. A mathematical theory of communication. *The Bell system technical journal* **1948**, *27*, 379–423.

(152) Bose, S. N. Planck's law and the hypothesis of light quanta. *Z. Phys* **1924**, *26*, 1–5.

(153) Zannoni, A. On the quantization of the monoatomic ideal gas. *arXiv preprint cond-mat/9912229* **1999**.

(154) Fermi, E. On quantizing an ideal monatomic gas. *Rend. Lincei* **1926**, *145*, 1–9.

(155) DeMarco, B.; Jin, D. S. Onset of Fermi degeneracy in a trapped atomic gas. *science* **1999**, *285*, 1703–1706.

(156) Dirac, P. A. M. On the theory of quantum mechanics. *Proceedings of the Royal Society of London. Series A, Containing Papers of a Mathematical and Physical Character* **1926**, *112*, 661–677.

(157) Planck, M. The theory of heat radiation. *Entropie* **1900**, *144*, 164.

(158) Tetrode, H. Die chemische Konstante der Gase und das elementare Wirkungsquantum. *Annalen der Physik* **1912**, *343*, 434–442.

(159) Sackur, O. Die Anwendung der kinetischen Theorie der Gase auf chemische Probleme. *Annalen der Physik* **1911**, *341*, 958–980.

(160) Sackur, O. Die universelle Bedeutung des sog. elementaren Wirkungsquantums. *Annalen der Physik* **1913**, *345*, 67–86.

(161) Nataraj, C. M.; van de Walle, A.; Samanta, A. Temperature-dependent configurational entropy calculations for refractory high-entropy alloys. *Journal of Phase Equilibria and Diffusion* **2021**, *42*, 571–577.